JOURNAL OF GUIDANCE, CONTROL, AND DYNAMICS
Vol. 34, No. 3, May–June 2011

Time-Efficient Angular Steering Laws for Rigid Satellites

Dov Verbin* and Vaios J. Lappas†
University of Surrey, Guildford, England GU2 7XH, United Kingdom
and
Joseph Z. Ben-Asher‡
Technion—Israel Institute of Technology, 32000 Haifa, Israel

DOI: 10.2514/1.48154

This paper proposes a new integrative control logic for rapid maneuvering of a rigid satellite using reaction wheels. The proposed control algorithm is of a state feedback nature and is designed to accommodate a variety of conditions, such as the general three-dimensional direction of rotation, initial and/or final angular rates, general alignment of three or four reaction wheels, torque and angular rate limits, and system time response limits. Simulations indicate that the new algorithm allows smooth control, free of chattering. The new controller also uses a tuning capability to compensate for time delays and parasitic dynamics. The tuning capability can be varied in order to enhance performance or robustness. Robustness of the algorithm is proven through a stability analysis and supported by detailed and practical simulations.

Nomenclature

BF(B)	=	body frame fixed to the satellite
F_α	=	ratio between safe and maximum acceleration; $0 < F_\alpha \leq 1$
F_ω	=	ratio between safe and maximum angular rate; $0 < F_\omega \leq 1$
h_{Wi}	=	angular momentum of ith reaction wheels, N · m · s
$\mathbf{H}^{\mathbf{S}}_{\mathbf{B}}$	=	total angular momentum of satellite including reaction wheels, as formulated in the body frame coordinates, N · m · s
IF(I)	=	inertial frame
$\mathbf{I_B}$	=	satellite moment of inertia with all reaction wheels at rest, Kg · m^2
$\mathbf{J}$	=	satellite 3 × 3 inertia matrix with all reaction wheels free to rotate around their axes, Kg · m^2
J_{Wi}	=	moment of inertia of ith reaction wheels, Kg · m^2
$\mathbf{q}$	=	quaternion vector of body frame relative to target frame
$\mathbf{S}_{\boldsymbol{\alpha}}$	=	matrix with each column defining two opposite surfaces of the angular acceleration envelope, s^2/rad
$\mathbf{S}_{\boldsymbol{\omega}}$	=	matrix with each column defining two opposite surfaces of the angular rate envelope, s/rad
t	=	time, s
TF(T)	=	target frame as an orthogonal right-handed frame defined to rotate at a constant angular rate relative to the inertial frame
$\|\mathbf{u}\|_\alpha$	=	angular acceleration norm of vector $\mathbf{u}$
$\|\mathbf{u}\|_\omega$	=	angular rate norm of vector $\mathbf{u}$
$\lceil \mathbf{u}, \mathbf{b} \rceil_\alpha$	=	biased angular acceleration envelope operator of vector $\mathbf{u}$ and bias $\mathbf{b}$
$\lceil \mathbf{u}, \mathbf{b} \rceil_\omega$	=	biased angular rate envelope operator of vector $\mathbf{u}$ and bias $\mathbf{b}$
$\mathbf{X_{orb}}$	=	vector of satellite orbital location and velocity in an inertial Earth-centered frame
$\boldsymbol{\alpha}_\mathbf{C}$	=	angular acceleration created by control actuators, rad/s^2
$\boldsymbol{\alpha}_\mathbf{D}$	=	angular acceleration disturbance caused by external sources, rad/s^2
$\boldsymbol{\theta}$	=	satellite angular position relative to target frame expressed as an Euler vector, rad
$\boldsymbol{v}_i$	=	unit vector in direction of ith reaction wheels rotation axis
$\boldsymbol{\tau}_\mathbf{E}$	=	total external torque acting on the satellite, as formulated in the body frame coordinates, N · m
τ_{Limit_i}	=	limit on absolute value of τ_{Wi}, N · m
τ_{Wi}	=	net torque acting on ith reaction wheels about its rotation axis, N · m (produced by reaction wheels motor)
$\boldsymbol{\omega}$	=	angular rate of body frame relative to target frame, with respect to body frame, rad/s; $\boldsymbol{\omega}_B^{B-T}$
ω_{Limit_i}	=	absolute value limit of ω_{Wi}, rad/s
ω_{Wi}	=	angular rate of ith reactions wheels relative to satellite body, rad/s
$\boldsymbol{\omega}_c^{a-b}$	=	angular rate vector of frame a relative to b frame, with respect to c frame, rad/s

I. Introduction

THIS work addresses the design of an efficient control logic for rapid rotational maneuvering of a rigid satellite equipped with reaction wheels (RWs). The RWs are fixed to the satellite structure. Their alignment is specific to each design, but at least three of them are assumed to be installed with their spin axes in three linearly independent directions to provide three-axis controllability. The use of four RWs is common [1] and provides redundancy as well as enhanced control capability. A common requirement with four-RW configurations is that each subset of three should provide three-axis controllability. Each RW's torque and angular rate are assumed to be limited symmetrically (equal limits in both directions) and separately (no link between the torque limit and the actual speed). It is also assumed that full knowledge of the system state (i.e., rotational state and angular rates of the satellite and angular rates of each RW) is available to the controller at any sampling point.

The subject of rigid satellite rotational maneuvering has been addressed extensively in literature. References [2,3] analyze the optimal control problem of minimum time angular maneuvers. It is first shown in [2] that the minimum time rotation with torque limited actuators is not necessarily along the Euler axis. Yet, in many cases, the Euler-axis rotation time is not very far from optimal. Reference [2] presents a comparison example of maneuvering times between time-optimal and Euler-axis time-optimal maneuvers with

Received 17 November 2009; revision received 13 September 2010; accepted for publication 20 December 2010. Copyright © 2010 by Dov Verbin. Published by the American Institute of Aeronautics and Astronautics, Inc., with permission. Copies of this paper may be made for personal or internal use, on condition that the copier pay the $10.00 per-copy fee to the Copyright Clearance Center, Inc., 222 Rosewood Drive, Danvers, MA 01923; include the code 0731-5090/11 and $10.00 in correspondence with the CCC.

*Ph.D. Candidate, Surrey Space Centre; Chief Attitude Control Engineer, Israel Aerospace Industries, MBT Space Division, 56000 Yehud, Israel.
†Senior Lecturer, Surrey Space Centre.
‡Professor, Faculty of Aerospace Engineering.

Table 1 Comparison example between time-optimal to Euler-axis time-optimal maneuvers [2]

Maneuver span, °	Time reduction, %
180	8.5
135	6.0
90	3.4
73	2.4
45	1.3
10	0.26
1	0.03

equal control capability along each of the three principal axes, as shown in Table 1.

The following references present various forms of closed-loop solutions. Reference [4] considers a three-axes system where the angular acceleration and angular rate limits are not reached. The paper proves the global stability for a three-axis proportional plus differential (PD) controller, where the angular error is the quaternion vector rather than the Euler vector that is used in this paper. Reference [1] presents a nonlinear state feedback design approach for Euler-axis maneuvers. A general four-RW configuration is assumed, and the redundancy (four RWs vs three rotation axes) is solved by minimizing the sum of squares of the RW torque control signals. Reference [5] suggests a real-time implementation of the open-loop solution of [2]. The controller is based on the approximate calculation of the switching times for the torque direction for each of the three RWs. The drawback of this solution is that an error in the switching time results in a final attitude error. The four-RW configuration is not considered in this paper. References [6–8] analyze maneuvers with system limits (angular acceleration, angular rate, and actuation time response). They suggest a solution for three-dimensional (3-D) time-optimal Euler-axis reorientation using thrusters and/or RWs. In all these techniques, the maneuver trajectories as well as the switching points are calculated in advance as functions of time (as in [6,8]) or as functions of the angular error (as in [7]). Only a simple orthogonally aligned three-RW configuration is considered in these papers. References [9,10] present a state-dependent closed-loop PD-like controller, using state-dependent gains for the single-axis near-time-optimal control of a system with angular acceleration limits. These studies do not consider actuation time response limits. In simulation results presented in [10], control chattering is evident and can be attributed to excessive gains in the presence of actuation time response limits. Reference [11] presents a complete controller for the maneuvering of the Infrared Astronomical Satellite (IRAS) (launched January 1983). The controller is designed for three-axis control. However, the maneuver is achieved only in one of the satellite's principal axes. In the IRAS case, the solution for efficient maneuvering is based on a real-time attitude command generator that produces the optimal trajectories and a linear regulator that allows the satellite to track these trajectories. The command generator is relatively simple, since it only deals with single-axis maneuvers. References [12,13] present techniques that are based on the variable structure control (VSC) method. The general conclusion from these two papers is that the VSC method with the linear switching surfaces cannot provide time-optimal or near-time-optimal control. Instead, the controllers use a regulator that enables the satellite to track optimal reference trajectories, as calculated by a time-optimal command generator. Reference [14] treats a three-axis system with angular rates and angular accelerations that are at levels below their limiting values. The paper suggests a control method to keep the rotation axis constant in the presence of disturbances and uncertainties. This proposed solution draws unnecessary power when the initial angular rate does not coincide with the initial rotation. Reference [15] proposes a cascaded control law with saturation logic, where the braking curve determines the desired 3-D angular rate for a given rotational state. This curved shape depends on the control capability in a given direction. Once this curve has been tracked, the satellite attitude and angular rate return to the origin at a specified safe angular rate and angular deceleration.

Following [1,15], the present paper takes the three-axis nonlinear state feedback approach that uses no reference trajectories and no precalculated switching times. The work presented in this paper is based, to a large extent, on [15]. However, the approach is different than [15] in several major aspects:

1) General actuator alignments (not necessarily one per principal axis) can be selected.

2) The control law applies a general mathematic method of defining the actuator's 3-D capability.

3) Additional terms are introduced in the controller to improve performance and enable the braking-curve tracking stability to be analytically proven.

4) The controller integral term is omitted.

5) The actuator's saturation occurrence is managed differently in order to improve the performance and analytically support the state convergence into the braking curve.

6) The Euler vector, rather than the quaternion vector, is employed in the control equations to allow a simpler and more accurate definition of the braking-curve shape.

7) The braking-curve angular rate is always in the direction of the Euler axis at each given time.

The aim of this paper is to develop an enhanced RW controller, using a practical integrative design approach, that will address a variety of possible conditions and limits in a combined manner. Particularly, the controller is designed to satisfy the following objectives:

1) The time for the rest-to-rest maneuver with zero momentum bias shall be as close to the eigenaxis (smallest possible angle) time-optimal rotation as the system bandwidth and the disturbance torque range may allow.

2) The controller shall be applicable to any three-RW or four-RW configurations that allow three-axes controllability, where each RW is torque limited.

3) The controller shall be applicable to any 3-D angular rate limiting envelope that can be expressed as $\|\boldsymbol{\omega}\|_{\omega} \leq 1$, where $\|\ \|_{\omega}$ represents a norm function satisfying the basic properties expressed in Eqs. (18–21).

4) The control torque shall be free of chattering along the maneuver.

5) The controller shall be state dependent and time independent, and it will not require a predefined reference attitude.

6) Any initial angular rate within the limit envelope shall be allowed.

7) Any final angular rate within the limit envelope shall be allowed.

The paper is structured as follows. Section II presents the equations of motion. Section III includes a review of the control allocation theory used in developing closed-form expressions for the angular acceleration and angular rate capability of the satellite with three RWs and four RWs. The formulation of the new control laws, along with a stability analysis, is presented in Sec. IV. Numerical examples and simulation results are presented in Sec. V, which demonstrate the improved control performance and tuning features.

II. Spacecraft Equations of Motion

The rigid satellite rotational equations can be expressed mathematically by the dynamics and kinematics equations. Equation (1) splits the angular acceleration between the controlled term $\boldsymbol{\alpha}_{\mathbf{C}}$, which is created by the RWs motor torques, and the disturbance term $\boldsymbol{\alpha}_D$, to be detailed along this section. Equation (2) is the Euler vector conversion of the quaternion kinematics equation from [6], $\dot{\mathbf{q}} = (1/2)[\cos(\theta/2)\boldsymbol{\omega} - \boldsymbol{\omega} \times \mathbf{q}]$, using the Euler vector definition, $\boldsymbol{\theta} \equiv \mathbf{q}[\theta/\sin(\theta/2)]$:

$$\dot{\boldsymbol{\omega}} = \boldsymbol{\alpha}_{\mathbf{C}} + \boldsymbol{\alpha}_{\mathbf{D}}(\boldsymbol{\theta}, \boldsymbol{\omega}, \mathbf{X}_{\mathbf{orb}}) \tag{1}$$

$$\dot{\boldsymbol{\theta}} = \boldsymbol{\omega} + \frac{1}{2}\boldsymbol{\theta} \times \boldsymbol{\omega} + \frac{2\tan(\theta/2) - \theta}{2\theta^2 \tan(\theta/2)}\boldsymbol{\theta} \times (\boldsymbol{\theta} \times \boldsymbol{\omega}) \tag{2}$$

Note that Eq. (2) reduces to $\dot{\boldsymbol{\theta}} = \boldsymbol{\omega}$ when $\boldsymbol{\omega}$ and $\boldsymbol{\theta}$ coincide, which implies rotation around the Euler (eigen) axis. Such a linear relation

for large rotation angles does not exist with the quaternion vector. This is the main reason for using the Euler vector in this work.

It is normally assumed that θ is bounded by $-\pi < \theta \leq \pi$, since there is no practical sense in rotating more than 180 deg when it is possible to rotate by a smaller angle in the opposite direction (unless the angle is close to the bound and the initial angular rate is in the same direction).

The following subsections expand on the dynamics of a rigid satellite equipped with RWs. The equations are based on [16] and are consistent with [6].

A. Reaction Wheels Equations

Each RW is assumed to be a perfectly balanced rotating body, such that its rotation does not affect the system mass properties. The ith RW angular momentum around its axis is calculated as follows:

$$h_{Wi} \equiv J_{Wi}(\boldsymbol{v}_i^T \boldsymbol{\omega}_B^{B-I} + \omega_{Wi}) \tag{3}$$

Where h_{Wi} responds to the RW net axial torque according to the following differential equation:

$$\frac{\mathrm{d}}{\mathrm{d}t} h_{Wi} = \tau_{Wi} \tag{4}$$

B. Rigid-Body Equations

Since the RWs are free to rotate about one axis, but in the other two axes, they are part of the rigid vehicle, parts of their mass shall be included in the rigid vehicle total moment of inertia. For this purpose, two moments of inertia for the satellite are defined: $\mathbf{I_B}$ with nonrotating RWs and $\mathbf{J}$ with free rotating RWs. The relation between the two is given by the following equation, where N is the number of RWs:

$$\mathbf{J} = \mathbf{I_B} - \sum_{i=1}^{N} J_{Wi} \boldsymbol{v}_i \boldsymbol{v}_i^T \tag{5}$$

The total angular momentum and the total control angular acceleration with N RWs are defined as follows, where $\boldsymbol{\omega}_{\mathbf{B}}^{\mathbf{B-I}}$ represents the vehicle inertial angular rate in the body frame (BF).

For the satellite system angular momentum,

$$\mathbf{H}_B^S \equiv \mathbf{J}\boldsymbol{\omega}_B^{B-I} + \sum_{i=1}^{N} \boldsymbol{v}_i h_{Wi} \tag{6}$$

For the control angular acceleration,

$$\boldsymbol{\alpha}_C \equiv -\mathbf{J}^{-1} \sum_{i=1}^{N} \boldsymbol{v}_i \tau_{Wi} \tag{7}$$

Since the time rate of change of the system angular momentum should be equal to the total external torque $\boldsymbol{\tau}_{\mathbf{E}}$ (resulting from aerodynamics, gravity gradient, magnetism, and solar pressure), we get

$$\boldsymbol{\tau}_{\mathbf{E}} = \left[\frac{\mathrm{d}}{\mathrm{d}t}\mathbf{H}^S\right]_I = \left[\frac{\mathrm{d}}{\mathrm{d}t}\mathbf{H}^S\right]_B + \boldsymbol{\omega}^{B-I} \times \mathbf{H}^S = \frac{\mathrm{d}}{\mathrm{d}t}\mathbf{H}_B^S + \boldsymbol{\omega}_B^{B-I} \times \mathbf{H}_B^S$$

Replacing terms from Eqs. (4), (6), and (7) into the preceding equation and rearranging the result gives

$$\frac{\mathrm{d}}{\mathrm{d}t}\boldsymbol{\omega}_B^{B-I} = \boldsymbol{\alpha}_{\mathbf{C}} + \mathbf{J}^{-1}(\boldsymbol{\tau}_{\mathbf{E}} - \boldsymbol{\omega}_B^{B-I} \times \mathbf{H}_B^S) \tag{8}$$

To meet the requirement to allow nonzero final angular rates, the vehicle angular rate $\boldsymbol{\omega}$ is defined here relative to a target frame (TF) that rotates at a constant angular rate relative to the inertial frame. This constant angular rate of TF is actually the final angular rate after the maneuver is completed. This leads to the following definition:

$$\boldsymbol{\omega} \equiv \boldsymbol{\omega}_B^{B-T} = \boldsymbol{\omega}_B^{B-I} - \boldsymbol{\omega}_B^{T-I} \tag{9}$$

Using Eqs. (8) and (9), the total angular acceleration disturbance is defined as follows:

$$\boldsymbol{\alpha}_{\mathbf{D}} \equiv \mathbf{J}^{-1}[\boldsymbol{\tau}_{\mathbf{E}} - (\boldsymbol{\omega} + \boldsymbol{\omega}_B^{T-I}) \times \mathbf{H}_B^S] + \boldsymbol{\omega} \times \boldsymbol{\omega}_B^{T-I} \tag{10}$$

It should be noted that, in practical control design, the control capability is always sufficiently large to counteract $\boldsymbol{\alpha}_{\mathbf{D}}$. There may be cases where it is necessary to limit the angular rate $\boldsymbol{\omega}$ during the maneuver such that $\boldsymbol{\alpha}_{\mathbf{D}}$ will not exceed the controllable level.

Following the preceding definitions and using Eqs. (8) and (9), the vehicle equation of motion becomes

$$\frac{\mathrm{d}}{\mathrm{d}t}\boldsymbol{\omega} = \boldsymbol{\alpha}_{\mathbf{C}} + \boldsymbol{\alpha}_{\mathbf{D}} \tag{11}$$

III. Control Allocation

This section analyzes and mathematically details the angular acceleration and angular rate resources and their links to the control allocation method. Section III.A is a review that is based on Sec. II.B of [17], and it is briefly presented for completeness. Section III.B presents a numerical comparison between two control allocation methods with the four-RW system. In Sec. III.C, the biased envelope operator (BEO) is introduced to model a nonsymmetric control capability, to be applied later in the new saturation management logic.

A. Review

1. Basic Control Allocation

The basic control allocation is the algorithm by which the control requirement in the BF level is translated to the RW level without considering the RW torque limits or angular rate limits. The control requirement may mean angular acceleration or angular rate. The angular acceleration demand is translated into RW torque, such that Eq. (7) is satisfied, and the angular rate demand is translated into RW angular momentum, such that Eq. (6) is satisfied (for a given $\mathbf{H}_B^S$). The basic control allocation task is to invert these equations. When only three RWs exist, the basic allocation is unique. However, in the case of four RWs or more, there may be an infinite number of solutions unless additional requirements exist, such as to optimize a certain cost function. Two common solutions are listed as follows:

1) The $L2$ solution minimizes the second norm of the N-dimensional RW control array; that is,

$$\mathrm{Min} \left\| \left[\frac{\tau_{W1}}{\tau_{\mathrm{Limit}_1}}, \frac{\tau_{W2}}{\tau_{\mathrm{Limit}_2}}, \frac{\tau_{W3}}{\tau_{\mathrm{Limit}_3}}, \ldots, \frac{\tau_{W_N}}{\tau_{\mathrm{Limit}_N}} \right] \right\|_2$$

2) The $L\infty$ solution minimizes the infinity norm of the N-dimensional RW control array; that is,

$$\mathrm{Min} \left\| \left[\frac{\tau_{W1}}{\tau_{\mathrm{Limit}_1}}, \frac{\tau_{W2}}{\tau_{\mathrm{Limit}_2}}, \frac{\tau_{W3}}{\tau_{\mathrm{Limit}_3}}, \ldots, \frac{\tau_{W_N}}{\tau_{\mathrm{Limit}_N}} \right] \right\|_\infty$$

In the case of angular rate allocation, the terms τ_{Wi} and τ_{Limit_i} are replaced in the preceding equations by h_{Wi} and $J_{Wi}\omega_{\mathrm{Limit}_i}$, and Eq. (7) is replaced by Eq. (6), where $\mathbf{H}_B^S$ can be regarded as a bias to be accounted for in the safety factor calculation [see Eq. (23) and Sec. III.A.3].

We define the basic allocation proportionality property as follows. If $[\tau_{W1}, \tau_{W2}, \tau_{W3,\ldots,} \tau_{W_N}]$ is allocated to $\boldsymbol{\alpha}_{\mathbf{C}}$, then for any scalar λ, $\lambda[\tau_{W1}, \tau_{W2}, \tau_{W3,\ldots,} \tau_{W_N}]$ will be allocated to $\lambda\boldsymbol{\alpha}_{\mathbf{C}}$. It can be easily shown that proportionality exists with $L2$, $L\infty$, and with any other norm-type cost function.

2. Definition of Control Norms

The control norm function is introduced to represent the system 3-D control capability. The 3-D control capability depends on the RW capabilities and on the basic control allocation algorithm, which is used to distribute the 3-D control between the RWs. Angular acceleration capability depends on the RW torque limit, and angular

rate capability may be dictated by the RW angular momentum limits or by the rate sensor measurement range. In the case of a limited rate sensor, the allocation will result in projecting the angular rate vector on the limited sensor sensitivity axes. With a given basic allocation method, the control norm function is defined as the maximum absolute value (over all the RWs) of the ratio between the basic allocated value and the RW limit value. The 3-D control capability is thus represented by all the admissible 3-D control vectors such that their control norm is smaller than or equal to unity. Note that, by this definition, the $L\infty$ method would always give the minimum norm.

Based on the previously stated proportionality claim, it is obvious that by dividing the control requirement by its norm, at least one RWs allocation would be on the limit, whereas the remainder would not be saturated. The control norm thus measures the proportion between the required control and the achievable control in the specified direction for the given basic allocation method. These norm functions, when operated on a general 3-D vector, give the ratio between the vector Euclidian magnitude and the maximum achievable angular acceleration or rate along the vector direction.

The angular acceleration norm will be denoted as $\|\mathbf{u}\|_\alpha$, and the angular rate norm will be denoted as $\|\mathbf{u}\|_\omega$, where $\mathbf{u}$ represents a general 3-D vector. Their algebraic definitions are as follows:

$$\|\mathbf{u}\|_\alpha \equiv \frac{\|\mathbf{u}\|_2}{\alpha_{\mathrm{Max}}(\mathbf{u})} \tag{12}$$

$$\|\mathbf{u}\|_\omega \equiv \frac{\|\mathbf{u}\|_2}{\omega_{\mathrm{Max}}(\mathbf{u})} \tag{13}$$

Thus,

$$\boldsymbol{\alpha}_{\mathrm{Max}}(\mathbf{u}) = \mathbf{u}\frac{1}{\|\mathbf{u}\|_\alpha} \tag{14}$$

$$\boldsymbol{\omega}_{\mathrm{Max}}(\mathbf{u}) = \mathbf{u}\frac{1}{\|\mathbf{u}\|_\omega} \tag{15}$$

Equation (14) defines the angular acceleration envelope, whereas Eq. (15) defines the angular rate envelope.

The following two expressions present the general control norms structure, typical to RW-controlled satellites. Derivation of the explicit norm formulas for three-RW- and four-RW-$L\infty$ systems can be found in [17]:

$$\|\mathbf{u}\|_\alpha = \|\mathbf{S}_{\boldsymbol{\alpha}}^T\mathbf{u}\|_\infty \tag{16}$$

$$\|\mathbf{u}\|_\omega = \|\mathbf{S}_{\boldsymbol{\omega}}^T\mathbf{u}\|_\infty \tag{17}$$

In the preceding equations, each column of the matrices $\mathbf{S}_{\boldsymbol{\alpha}}$ and $\mathbf{S}_{\boldsymbol{\omega}}$ is a 3-D vector that defines two opposite planar faces of the multiplane shape of the angular acceleration and angular rate envelopes. Each component of $\mathbf{S}^T\mathbf{u}$ is, in fact, a basic allocation result for one or more RWs, and the maximum absolute value is taken according to the norm definition that was given in Sec. III.A.2. It can be easily verified that functions (16) and (17) satisfy all of the four properties required for a norm; that is,

$$\|\mathbf{0}\| = 0 \tag{18}$$

$$\|\mathbf{u}\| > 0 \qquad \text{for every } \mathbf{u} \neq \mathbf{0} \tag{19}$$

$$\|\mathbf{u}\lambda\| = \|\mathbf{u}\||\lambda| \qquad \text{for every scalar } \lambda \tag{20}$$

$$\|\mathbf{u}\| + \|\mathbf{v}\| \geq \|\mathbf{u} + \mathbf{v}\| \tag{21}$$

3. Finding Safe Control Limits

Using Eqs. (14) and (15), the maximum control in a given direction of a general vector $\mathbf{u}$ can be obtained. The following subsection explains how the maximum safe control can be selected in a way that allows a required margin for disturbance compensation or bias rate (e.g., nonzero rate of TF). This is translated as follows:

$$\|\boldsymbol{\alpha}_{\mathbf{Safe}}(\mathbf{u}) + \boldsymbol{\alpha}_{\mathbf{D}}\|_\alpha \leq 1 \tag{22}$$

$$\|\boldsymbol{\omega}_{\mathbf{Safe}}(\mathbf{u}) + \boldsymbol{\omega}_{\mathbf{Bias}}\|_\omega \leq 1 \tag{23}$$

The triangle inequality [Eq. (21)] gives

$$\|\boldsymbol{\alpha}_{\mathbf{Safe}}(\mathbf{u}) + \boldsymbol{\alpha}_{\mathbf{D}}\|_\alpha \leq \|\boldsymbol{\alpha}_{\mathbf{Safe}}(\mathbf{u})\|_\alpha + \|\boldsymbol{\alpha}_{\mathbf{D}}\|_\alpha \tag{24}$$

$$\|\boldsymbol{\omega}_{\mathbf{Safe}}(\mathbf{u}) + \boldsymbol{\omega}_{\mathbf{Bias}}\|_\omega \leq \|\boldsymbol{\omega}_{\mathbf{Safe}}(\mathbf{u})\|_\omega + \|\boldsymbol{\omega}_{\mathbf{Bias}}\|_\omega \tag{25}$$

Thus, referring again to Eqs. (22) and (23),

$$\|\boldsymbol{\alpha}_{\mathbf{Safe}}(\mathbf{u})\|_\alpha + \|\boldsymbol{\alpha}\| \leq 1\mathbf{D} \tag{26}$$

$$\|\boldsymbol{\omega}_{\mathbf{Safe}}(\mathbf{u})\|_\omega + \|\boldsymbol{\omega}_{\mathbf{Bias}}\|_\omega \leq 1 \tag{27}$$

Now, the safety factors are defined as follows:

$$F_\alpha \equiv 1 - \mathrm{Max}\{\|\boldsymbol{\alpha}_{\mathbf{D}}\|_\alpha\} \tag{28}$$

$$F_\omega \equiv 1 - \mathrm{Max}\{\|\boldsymbol{\omega}_{\mathbf{Bias}}\|_\omega\} \tag{29}$$

It is assumed that both F_α and F_ω are positive, because negative values would indicate the possibility of the disturbance being in excess of the available control. The equations of safe angular acceleration and safe angular rate in the direction of $\mathbf{u}$ can now be further developed. First, a positive λ is defined, such that $\boldsymbol{\alpha}_{\mathbf{Safe}}(\mathbf{u}) = \lambda\mathbf{u}$. Substituting into Eq. (26) and using Eq. (28) results in $\|\lambda\mathbf{u}\|_\alpha = F_\alpha$. Using Eq. (20) gives $\lambda = F_\alpha/\|\mathbf{u}\|_\alpha$. Therefore,

$$\boldsymbol{\alpha}_{\mathbf{Safe}}(\mathbf{u}) = \mathbf{u}\frac{F_\alpha}{\|\mathbf{u}\|_\alpha} \tag{30}$$

and, similarly,

$$\boldsymbol{\omega}_{\mathbf{Safe}}(\mathbf{u}) = \mathbf{u}\frac{F_\omega}{\|\mathbf{u}\|_\omega} \tag{31}$$

B. Numerical Comparison Between *L2* to *L*∞ Allocation Methods

The comparison case presented uses the symmetrically aligned four-RW configuration according to Fig. 1, where X_{Wi} denotes the rotation axis of the RW, and the angles refer to the projections on the page plane.

The numerical values for this example are

$$\mathbf{J} = \begin{pmatrix} 70 & 0 & 0 \\ 0 & 90 & 0 \\ 0 & 0 & 120 \end{pmatrix} \mathrm{Kg}\cdot\mathrm{m}^2; \qquad \beta = 30^\circ, \qquad \delta = 30^\circ;$$

$$\tau_{\mathrm{Limit}_i} = 0.5\ \mathrm{N}\cdot\mathrm{m} \quad \text{for } i = 1, \ldots, 4$$

For the $L\infty$ allocation, the solution presented in Eqs. (2–30) of [17] is used. For the $L2$, the allocation logic of [1] is followed. Figure 2 compares the maximum angular acceleration 3-D envelope of the $L2$ and $L\infty$ methods in four cross sections parallel to the X_B-Y_B plane. It is clear from Fig. 2 that the $L\infty$ envelope contains more volume. The calculation demonstrates that the advantage at a given control direction varies from zero on the principal planes up to 50% on the corners of the middle cross section ($0.5 \times 0.046\ \mathrm{rad/s}^2$).

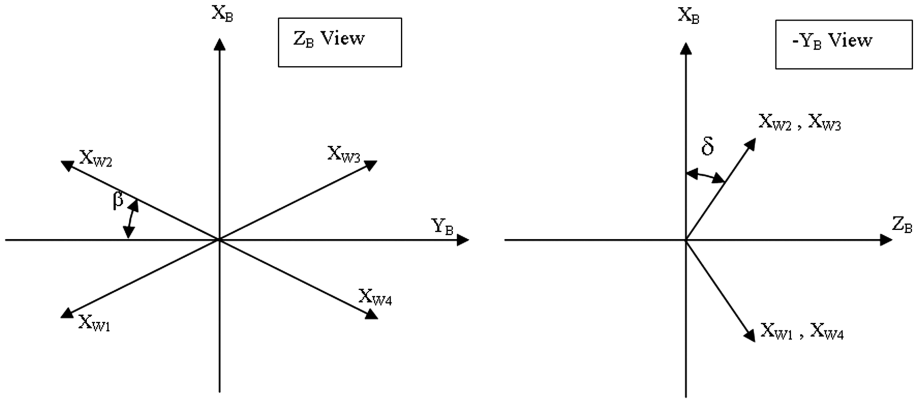

Fig. 1 Numerical example of RW alignment.

C. Biased Envelope Operator

Normalizing the control vector, as in Eqs. (14) and (15), makes it possible to get the maximum control in the given direction. However, there may be cases (presented in the next section) where the control is the sum of two components: the first of which has to be normalized, whereas the second should not be changed. This second component is denoted here as the bias. The goal is to find the factor to divide the first component by, such that the resulting norm would be equal to the safety factor, as illustrated in Fig. 3.

The BEO for a vector $\mathbf{u}$ with bias $\mathbf{b}$ will be denoted as $\lceil \mathbf{u}, \mathbf{b} \rceil_\alpha$ for angular acceleration and $\lceil \mathbf{u}, \mathbf{b} \rceil_\omega$ for angular rate, and it is defined to be the positive solution that satisfies

$$F_\alpha = \left\| \frac{\mathbf{u}}{\lceil \mathbf{u}, \mathbf{b} \rceil_\alpha} + \mathbf{b} \right\|_\alpha \tag{32}$$

$$F_\omega = \left\| \frac{\mathbf{u}}{\lceil \mathbf{u}, \mathbf{b} \rceil_\omega} + \mathbf{b} \right\|_\omega \tag{33}$$

The explicit form for $\lceil \mathbf{u}, \mathbf{b} \rceil$ is developed in the rest of this subsection for both the angular acceleration and rate. For convenience and clarity, the subscripts α and ω, for angular acceleration and angular rate, respectively, are omitted.

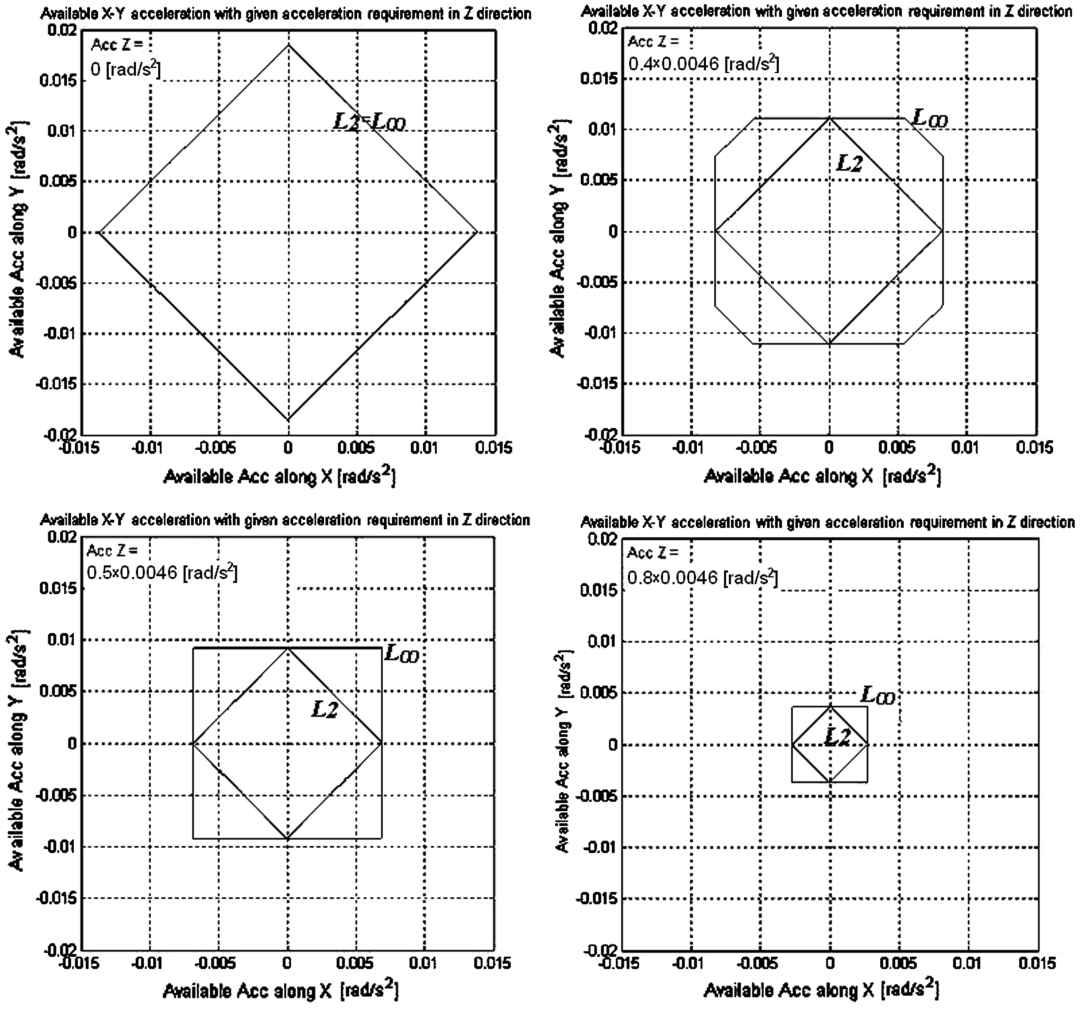

Fig. 2 Comparison between control allocation algorithms *L2* and *L*∞ (Acc denotes acceleration).

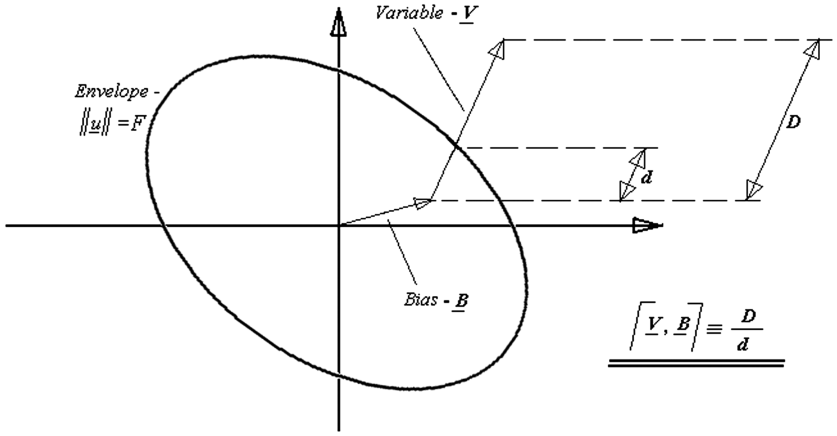

Fig. 3 BEO diagram.

Equations (16) and (17) may be rewritten, replacing the absolute value operation according to the identity $|x| = \text{Max}\{-x, +x\}$:

$$\|\mathbf{u}\| = \text{Max}\left\{\begin{pmatrix}\mathbf{S}^T\\ -\mathbf{S}^T\end{pmatrix}\mathbf{u}\right\} \tag{34}$$

Substituting Eq. (34) in Eq. (32) or Eq. (33) results in

$$F = \text{Max}\left\{\begin{pmatrix}\mathbf{S}^T\\ -\mathbf{S}^T\end{pmatrix}\left(\mathbf{b} + \mathbf{u}\frac{1}{\lceil \mathbf{u}, \mathbf{b}\rceil}\right)\right\} \tag{35}$$

Using the index i for each column of $\mathbf{S}$ and combining terms gives

$$F = \text{Max}_i\left\{\text{Max}\left[\mathbf{S}_i^T\mathbf{b} + \frac{\mathbf{S}_i^T\mathbf{u}}{\lceil \mathbf{u}, \mathbf{b}\rceil}, -\mathbf{S}_i^T\mathbf{b} - \frac{\mathbf{S}_i^T\mathbf{u}}{\lceil \mathbf{u}, \mathbf{b}\rceil}\right]\right\} \tag{36}$$

For a given i, and ignoring the Max, two possible solutions for $\lceil \mathbf{u}, \mathbf{b}\rceil$ exist:

$$\lceil \mathbf{u}, \mathbf{b}\rceil(i) = \frac{\mathbf{S}_i^T\mathbf{u}}{F - \mathbf{S}_i^T\mathbf{b}}, \qquad \frac{-\mathbf{S}_i^T\mathbf{u}}{F + \mathbf{S}_i^T\mathbf{b}} \tag{37}$$

A validity condition for the BEO is $\|\mathbf{b}\| < F$: i.e., the bias shall not exceed the control capability. This implies that $|\mathbf{S}_i^T\mathbf{b}| < F$ for any i. Therefore, the denominators of both terms in Eq. (37) are always positive, such that the two solutions are of opposite signs. By the BEO definition, only the positive solution is chosen. This implies that if $\mathbf{S}_i^T\mathbf{u}$ is positive, then the first solution shall be selected, and if not, the second shall be selected. Note that once the solution satisfying the equality with F is selected, the other (nonselected) term in Eq. (36) would always be negative and equal to $-F$, which justifies its elimination.

A general expression for the positive solution between the two is

$$\lceil \mathbf{u}, \mathbf{b}\rceil(i) = \frac{|\mathbf{S}_i^T\mathbf{u}|}{F - \text{sign}(\mathbf{S}_i^T\mathbf{u})\mathbf{S}_i^T\mathbf{b}} \tag{38}$$

It can be observed that choosing the maximum value of the preceding equation at a particular index i will satisfy Eq. (36), since all other instances of Eq. (36) with different i will always be smaller or equal to this value. This is true, because the numerator $\pm\mathbf{S}_i^T\mathbf{u}$ of the noneliminated term in Eq. (36) must always be positive when the validity condition $|\mathbf{S}_i^T\mathbf{b}| < F$ is satisfied.

The solution to $\lceil \mathbf{u}, \mathbf{b}\rceil$ is thus summarized in the following equations (again with the subscripts α or ω).

For angular acceleration,

$$\lceil \mathbf{u}, \mathbf{b}\rceil_\alpha = \text{Max}_i\left\{\frac{|(\mathbf{S}_\alpha)_i^T\mathbf{u}|}{F_\alpha - \text{sign}[(\mathbf{S}_\alpha)_i^T\mathbf{u}](\mathbf{S}_\alpha)_i^T\mathbf{b}}\right\} \tag{39}$$

For angular rate,

$$\lceil \mathbf{u}, \mathbf{b}\rceil_\omega = \text{Max}_i\left\{\frac{|(\mathbf{S}_\omega)_i^T\mathbf{u}|}{F_\omega - \text{sign}[(\mathbf{S}_\omega)_i^T\mathbf{u}](\mathbf{S}_\omega)_i^T\mathbf{b}}\right\} \tag{40}$$

Finally, following Eqs. (32) and (33), the terms for the maximum (where $F = 1$) or safe (where $0 < F < 1$) controls in the direction of $\mathbf{u}$ are as follows.

For angular acceleration,

$$\boldsymbol{\alpha}_{\mathbf{Safe}}(\mathbf{u}, \mathbf{b}) = \mathbf{u}\frac{1}{\lceil \mathbf{u}, \mathbf{b}\rceil_\alpha} \tag{41}$$

For angular rate,

$$\boldsymbol{\omega}_{\mathbf{Safe}}(\mathbf{u}, \mathbf{b}) = \mathbf{u}\frac{1}{\lceil \mathbf{u}, \mathbf{b}\rceil_\omega} \tag{42}$$

IV. Control Law

The main goal of the control law is to change the system state $\{\boldsymbol{\theta}, \boldsymbol{\omega}\}$ from any initial value $\{\boldsymbol{\theta}_0, \boldsymbol{\omega}_0\}$ to $\{\mathbf{0}, \mathbf{0}\}$, while the control and the state stay within the specified system limits. Additionally, the control law should aim for time efficiency and smoothness, as listed in Sec. I. Rapid response is the primary performance objective, but it can be interchanged in the approach developed here for algorithm simplicity and control smoothness.

The suggested control has a cascaded structure as follows:

$$\boldsymbol{\alpha}_{\mathbf{C}} = \omega_n[\mathbf{f}(\boldsymbol{\theta}) - \boldsymbol{\omega}] + \boldsymbol{\alpha}_{\mathbf{FF}} - \boldsymbol{\alpha}_{\mathbf{D}} \tag{43}$$

Where the input is the satellite rigid-body rotational state $\{\boldsymbol{\theta}, \boldsymbol{\omega}\}$, as related to TF, which is assumed to rotate at a constant angular rate. The output is the control angular acceleration vector $\boldsymbol{\alpha}_{\mathbf{C}}$, as defined in Eq. (7). The other notations are as follows:

1) The parameter ω_n is a scalar gain.

2) The function $\mathbf{f}(\boldsymbol{\theta})$ is the braking curve linking the desired angular rate to the angular position. It is a 3-D function for which the direction is precisely opposite to $\boldsymbol{\theta}$, and its magnitude is based on the eigenaxis time-optimal braking curve (as shown in Fig. 4) using the safe limits of acceleration and rate in the direction of $\boldsymbol{\theta}$. Note that choosing $\mathbf{f}(\boldsymbol{\theta})$ on the same line as $\boldsymbol{\theta}$ reduces Eq. (2) of the system kinematics to $\dot{\boldsymbol{\theta}} = \boldsymbol{\omega}$ (as long as the curve is tracked), and the direction of $\boldsymbol{\theta}$ (the Euler axis) would then be constant.

3) The variable $\boldsymbol{\alpha}_{\mathbf{FF}}$ is introduced to compensate for the rate of change of $\mathbf{f}(\boldsymbol{\theta})$ [see Eq. (45)].

4) The variable $\boldsymbol{\alpha}_{\mathbf{D}}$ is a term to compensate for the disturbance elements in Eq. (1). It is derived from Eq. (10).

In the remainder of this section, the controller is further developed, starting from the relevant stability theorems, then going through the formulation of explicit control equations and ending with the issue of control saturation management.

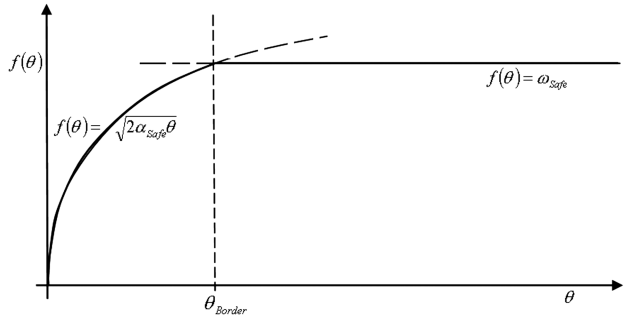

Fig. 4 Single-axis time-optimal braking curve $f(\theta)$.

A. Theorem A: Asymptotic Stability of Curve Tracking Error $\mathbf{f}(\boldsymbol{\theta})-\boldsymbol{\omega}$

Theorem A: With the control defined in Eq. (43), the curve tracking error $\mathbf{f}(\boldsymbol{\theta})-\boldsymbol{\omega}$ is asymptotically stable.

Proof: Replacing $\boldsymbol{\alpha}_{\mathbf{C}}$ in Eq. (11) with Eq. (43) and assuming that the disturbance $\boldsymbol{\alpha}_{\mathbf{D}}$ is fully compensated,

$$\frac{\mathrm{d}}{\mathrm{d}t}\boldsymbol{\omega}-\boldsymbol{\alpha}_{\mathbf{FF}}=\omega_n[\mathbf{f}(\boldsymbol{\theta})-\boldsymbol{\omega}] \tag{44}$$

Let $\boldsymbol{\alpha}_{\mathbf{FF}}$ be calculated to fulfill the following definition:

$$\boldsymbol{\alpha}_{\mathbf{FF}}\equiv\frac{\mathrm{d}}{\mathrm{d}t}[\mathbf{f}(\boldsymbol{\theta})] \tag{45}$$

Substituting into Eq. (44), the closed-loop differential equation becomes

$$\frac{\mathrm{d}}{\mathrm{d}t}[\boldsymbol{\omega}-\mathbf{f}(\boldsymbol{\theta})]=-\omega_n[\boldsymbol{\omega}-\mathbf{f}(\boldsymbol{\theta})] \tag{46}$$

This indicates stable braking-curve tracking dynamics with no coupling between the error components and three real stable poles at $-\omega_n$ each. The stable tracking can be tuned by using the ω_n parameter. To avoid controller chattering, an ω_n, which is compatible with the natural system delays, shall be appropriately chosen.

B. Theorem B: Alternative Conditions for Eigenaxis Direction Stability

Theorem B: The cross product $\boldsymbol{\omega}\times\boldsymbol{\theta}$ is asymptotically stable with any control that satisfies

$$\dot{\boldsymbol{\omega}}=-\boldsymbol{\theta}g_1-\boldsymbol{\omega}g_2 \tag{47}$$

Where g_1 and g_2 are any positive scalar variables, which may be functions of the state or time.

Two conclusions of this theorem are listed next:

1) When Eq. (47) is valid, either $\boldsymbol{\theta}$ and $\boldsymbol{\omega}$ will both converge to zero or their directions will converge to a single line (colinearity). Note that convergence of $\boldsymbol{\theta}$ alone or $\boldsymbol{\omega}$ alone cannot be steady when the control is active.

2) When Eq. (47) is valid, the colinearity of $\boldsymbol{\theta}$ and$\boldsymbol{\omega}$ is a stable situation.

Proof: By using Liapunov's stability theorem for a general system (as applied in [4]), we define a positive definite energy function P as

$$P=\frac{1}{2}\left(\frac{\mathrm{Sin}(\theta/2)}{\theta}\right)^2(\boldsymbol{\omega}\times\boldsymbol{\theta})^T(\boldsymbol{\omega}\times\boldsymbol{\theta}) \tag{48}$$

It is assumed that $|\theta|\le\pi$ (as mentioned in Sec. II), such that the multiplying scalar term in the energy function is always positive and bounded by $(1/\pi)^2\le(\mathrm{Sin}(\theta/2)/\theta)^2\le(1/2)^2$; thus, it does not change the positive definiteness of P.

It is now important to prove that the time derivative of P is negative for every $\boldsymbol{\omega}\times\boldsymbol{\theta}\neq\mathbf{0}$. Given that,

$$\mathbf{q}\equiv\boldsymbol{\theta}\frac{\mathrm{Sin}(\theta/2)}{\theta} \tag{49}$$

$$P=\tfrac{1}{2}(\boldsymbol{\omega}\times\mathbf{q})^T(\boldsymbol{\omega}\times\mathbf{q}) \tag{50}$$

The time derivative of $\mathbf{q}$ is given as follows [6]:

$$\dot{\mathbf{q}}=\tfrac{1}{2}\cos(\tfrac{\theta}{2})\boldsymbol{\omega}-\tfrac{1}{2}\boldsymbol{\omega}\times\mathbf{q} \tag{51}$$

Taking the time derivative from Eq. (50) results in

$$\dot{P}=(\boldsymbol{\omega}\times\mathbf{q})^T(\dot{\boldsymbol{\omega}}\times\mathbf{q})+(\boldsymbol{\omega}\times\mathbf{q})^T(\boldsymbol{\omega}\times\dot{\mathbf{q}}) \tag{52}$$

Taking $\dot{\mathbf{q}}$ from Eq. (51) and $\dot{\boldsymbol{\omega}}$ from Eq. (47) and substituting into Eq. (52) yields

$$\dot{P}=(\boldsymbol{\omega}\times\mathbf{q})^T[(-g_1\boldsymbol{\theta}-g_2\boldsymbol{\omega})\times\mathbf{q}]+(\boldsymbol{\omega}\times\mathbf{q})^T[\boldsymbol{\omega}\times(\tfrac{1}{2}\cos(\tfrac{\theta}{2})\boldsymbol{\omega}-\tfrac{1}{2}\boldsymbol{\omega}\times\mathbf{q})] \tag{53}$$

Now, replacing $\boldsymbol{\theta}\times\mathbf{q}=\mathbf{0}$ [Eq. (49)] in the first term, as well as using $\boldsymbol{\omega}\times\boldsymbol{\omega}=\mathbf{0}$ in the second term, gives

$$\dot{P}=-g_2(\boldsymbol{\omega}\times\mathbf{q})^T(\boldsymbol{\omega}\times\mathbf{q})-\tfrac{1}{2}(\boldsymbol{\omega}\times\mathbf{q})^T[\boldsymbol{\omega}\times(\boldsymbol{\omega}\times\mathbf{q})] \tag{54}$$

In Eq. (54), the second term on the right-hand side vanishes (a dot product between two normal vectors). Replacing the remaining term by Eq. (50) gives

$$\dot{P}=-2g_2P \tag{55}$$

This implies that $\dot{P}$ is negative for every $\boldsymbol{\omega}\times\boldsymbol{\theta}\neq\mathbf{0}$, which proves the asymptotic stability.

Moreover, the result of Eq. (55) implies that the time constant of the potential P convergence is $\tau=1/(2g_2)$.

C. Curve $\mathbf{f}(\boldsymbol{\theta})$

The curve $\mathbf{f}(\boldsymbol{\theta})$ is defined in six-dimensional state space $\{\boldsymbol{\theta},\boldsymbol{\omega}\}$. It sets the reference 3-D angular rate as a function of the 3-D attitude $\boldsymbol{\theta}$. The direction of $\mathbf{f}(\boldsymbol{\theta})$ is opposite to $\boldsymbol{\theta}$, and its magnitude follows the Euler-axis time-optimal braking curve, with limited angular rate and deceleration as presented in [1,2,6,7,9–11,15,18]. Therefore, $\mathbf{f}(\boldsymbol{\theta})$ is related to the single-axis braking curve by the following equation:

$$\mathbf{f}(\boldsymbol{\theta})=-f(\theta)\hat{\boldsymbol{\theta}} \tag{56}$$

Where $\hat{\boldsymbol{\theta}}$ is a unit vector in the direction of $\boldsymbol{\theta}$, and $f(\theta)$ is a positive scalar function of the magnitude of $\boldsymbol{\theta}$ and the limit angular rate and acceleration along $\boldsymbol{\theta}$, as illustrated in Fig. 4.

Note that substitution of the Euler angle θ in Fig. 4 with a quaternion vector component (as is done in [15]) might be a good approximation. However, the parabolic curve is accurate only for angular representation.

The mathematical expression of the curve $\mathbf{f}(\boldsymbol{\theta})$ is analyzed in the remainder of this subsection. The curve is split at θ_{Border} into two parts. The first is the parabolic curve determined by the angular acceleration limit, and the second is a horizontal line on the level of the angular rate limit. To develop the necessary expressions, $f(\theta)$ in Eq. (56) is replaced by the appropriate terms that appear in Fig. 4. This gives

$$\mathbf{f}(\boldsymbol{\theta})=-\sqrt{2\alpha_{\mathrm{Safe}}\theta}\hat{\boldsymbol{\theta}},\qquad\text{where }\theta<\theta_{\mathrm{Border}} \tag{57}$$

$$\mathbf{f}(\boldsymbol{\theta})=-\omega_{\mathrm{Safe}}\hat{\boldsymbol{\theta}},\qquad\text{where }\theta\ge\theta_{\mathrm{Border}} \tag{58}$$

Now, replacing according to Eqs. (30) and (31), $\alpha_{\mathrm{Safe}}(\boldsymbol{\theta})=(F_\alpha/\|\boldsymbol{\theta}\|_\alpha)\theta$, $\omega_{\mathrm{Safe}}(\boldsymbol{\theta})=(F_\omega/\|\boldsymbol{\theta}\|_\omega)\theta$, and $\hat{\boldsymbol{\theta}}\equiv\boldsymbol{\theta}(1/\theta)$ will give

$$\mathbf{f}(\boldsymbol{\theta}) = -\sqrt{\frac{2F_\alpha}{\|\boldsymbol{\theta}\|_\alpha}}\boldsymbol{\theta}, \qquad \text{where } \theta < \theta_{\text{Border}} \tag{59}$$

$$\mathbf{f}(\boldsymbol{\theta}) = -\frac{F_\omega}{\|\boldsymbol{\theta}\|_\omega}\boldsymbol{\theta}, \qquad \text{where } \theta \geq \theta_{\text{Border}} \tag{60}$$

D. Compensation Term $\boldsymbol{\alpha}_{\mathbf{FF}}$

The compensation term $\boldsymbol{\alpha}_{\mathbf{FF}}$ is calculated differently for each of the two parts of Fig. 4, as defined by θ_{Border}.

1) Angular acceleration is dominant: i.e., $\theta < \theta_{\text{Border}}$.

The following results from Eqs. (45) and (59) for the part of $\mathbf{f}(\boldsymbol{\theta})$ that conforms to the angular acceleration limit:

$$\boldsymbol{\alpha}_{\mathbf{FF}} = -\frac{\mathrm{d}}{\mathrm{d}t}\left[\sqrt{\frac{2F_\alpha}{\|\boldsymbol{\theta}\|_\alpha}}\boldsymbol{\theta}\right] = -\sqrt{\frac{F_\alpha}{2}}\left\{\frac{2\|\boldsymbol{\theta}\|_\alpha \frac{\mathrm{d}}{\mathrm{d}t}\boldsymbol{\theta} - \boldsymbol{\theta}\frac{\mathrm{d}}{\mathrm{d}t}\|\boldsymbol{\theta}\|_\alpha}{\|\boldsymbol{\theta}\|_\alpha^{3/2}}\right\} \tag{61}$$

To enable the calculation of the time derivative of $\|\boldsymbol{\theta}\|_\alpha$, Eq. (34) is used, and the surface vector $\mathbf{S}_i$ or $-\mathbf{S}_i$ that produces maximum $\mathbf{S}_i^T\mathbf{u}$ or $-\mathbf{S}_i^T\mathbf{u}$ is denoted by $\mathbf{Z}_m$, where $\mathbf{Z}_m$ may be equal either to $\mathbf{S}_m$ or to $-\mathbf{S}_m$, such that, as long as it is constant, it is possible to get

$$\|\boldsymbol{\theta}\|_\alpha = \mathbf{Z}_m^T\boldsymbol{\theta} \tag{62}$$

It is expected that $\mathbf{Z}_m$ would be (piecewise) constant over time, except for numbered switching occasions. Splitting the first term in the numerator of Eq. (61), $2\|\boldsymbol{\theta}\|_\alpha\dot{\boldsymbol{\theta}}$, into two equal parts and replacing $\|\boldsymbol{\theta}\|_\alpha$ according to Eq. (62) gives

$$\boldsymbol{\alpha}_{\mathbf{FF}} = -\sqrt{\frac{F_\alpha}{2}}\left\{\frac{\dot{\boldsymbol{\theta}}}{\sqrt{\|\boldsymbol{\theta}\|_\alpha}} + \frac{\dot{\boldsymbol{\theta}}(\mathbf{Z}_m^T\boldsymbol{\theta}) - \boldsymbol{\theta}(\mathbf{Z}_m^T\dot{\boldsymbol{\theta}})}{\|\boldsymbol{\theta}\|_\alpha^{3/2}}\right\} \tag{63}$$

Using the identity $(\mathbf{a}\times\mathbf{b})\times\mathbf{c} = \mathbf{b}(\mathbf{c}^\mathbf{T}\mathbf{a}) - \mathbf{a}(\mathbf{c}^\mathbf{T}\mathbf{b})$, Eq. (63) can be rewritten as follows:

$$\boldsymbol{\alpha}_{\mathbf{FF}} = -\sqrt{\frac{F_\alpha}{2}}\left\{\frac{\dot{\boldsymbol{\theta}}}{\sqrt{\|\boldsymbol{\theta}\|_\alpha}} + \frac{(\boldsymbol{\theta}\times\dot{\boldsymbol{\theta}})\times\mathbf{Z}_m}{\|\boldsymbol{\theta}\|_\alpha^{3/2}}\right\} \tag{64}$$

By applying Eq. (2), it is now possible to get a full explicit expression for $\boldsymbol{\alpha}_{\mathbf{FF}}$, which is included in the control law in Eq. (43). The expression contains the state variables $\boldsymbol{\theta}$ and $\boldsymbol{\omega}$ and the vector $\mathbf{Z}_m$ that is dependent on $\boldsymbol{\theta}$. However, it is proposed to simplify the preceding expression by taking advantage of Theorem B, which allows us to take a zero value for the cross product $\boldsymbol{\omega}\times\boldsymbol{\theta}$ when the controller satisfies the condition of Eq. (47).

By taking $\dot{\boldsymbol{\theta}}$ from Eq. (2) and eliminating all the occurrences of $\boldsymbol{\omega}\times\boldsymbol{\theta}$, Eq. (64) is reduced as follows:

$$\boldsymbol{\omega}\times\boldsymbol{\theta} \to \mathbf{0} \Rightarrow \boldsymbol{\alpha}_{\mathbf{FF}} = -\boldsymbol{\omega}\sqrt{F_\alpha/2\|\boldsymbol{\theta}\|_\alpha} \tag{65}$$

2) The angular rate is dominant: i.e., $\theta \geq \theta_{\text{Border}}$.

Using Eqs. (45) and (60), the time derivative of $\mathbf{f}(\boldsymbol{\theta})$, which conforms with the angular rate limit, is generated as follows:

$$\boldsymbol{\alpha}_{\mathbf{FF}} = -\frac{\mathrm{d}}{\mathrm{d}t}\left[\frac{F_\omega}{\|\boldsymbol{\theta}\|_\omega}\boldsymbol{\theta}\right] = -F_\omega\left\{\frac{\|\boldsymbol{\theta}\|_\omega\frac{\mathrm{d}}{\mathrm{d}t}\boldsymbol{\theta} - \boldsymbol{\theta}\frac{\mathrm{d}}{\mathrm{d}t}\|\boldsymbol{\theta}\|_\omega}{\|\boldsymbol{\theta}\|_\omega^2}\right\} \tag{66}$$

Repeating the same process as in the previous case gives

$$\boldsymbol{\alpha}_{\mathbf{FF}} = F_\omega\left\{\frac{\boldsymbol{\theta}(\mathbf{Z}_m^T\dot{\boldsymbol{\theta}}) - \dot{\boldsymbol{\theta}}(\mathbf{Z}_m^T\boldsymbol{\theta})}{(\mathbf{Z}_m^T\boldsymbol{\theta})^2}\right\} = \frac{F_\omega(\dot{\boldsymbol{\theta}}\times\boldsymbol{\theta})\times\mathbf{Z}_m}{(\mathbf{Z}_m^T\boldsymbol{\theta})^2} \tag{67}$$

Again, by applying Eq. (2) in Eq. (67) and eliminating all the occurrences of $\boldsymbol{\omega}\times\boldsymbol{\theta}$, the expression for $\boldsymbol{\alpha}_{\mathbf{FF}}$ is simplified. It can thus be summarized that whenever $\boldsymbol{\omega}\times\boldsymbol{\theta} \to \mathbf{0}$, $\boldsymbol{\alpha}_{\mathbf{FF}}$ is given as follows:

$$\boldsymbol{\alpha}_{\mathbf{FF}} = -\boldsymbol{\omega}\sqrt{\frac{F_\alpha}{2\|\boldsymbol{\theta}\|_\alpha}} \tag{68}$$

for the angular acceleration limit case, and

$$\boldsymbol{\alpha}_{\mathbf{FF}} = 0 \tag{69}$$

for the angular rate limit case.

Note that these results, together with the general control structure of Eq. (43) and the choice of $\mathbf{f}(\boldsymbol{\theta})$ on the same line as $\boldsymbol{\theta}$, assure that the condition expressed by Eq. (47) is indeed satisfied.

E. Explicit Controller Equations

Replacing the results from Eqs. (59) and (60) for $\mathbf{f}(\boldsymbol{\theta})$ and Eqs. (68) and (69) for $\boldsymbol{\alpha}_{\mathbf{FF}}$ into Eq. (43) results in

$$\boldsymbol{\alpha}_{\mathbf{C}} = -\omega_n\left[\sqrt{\frac{2F_\alpha}{\|\boldsymbol{\theta}\|_\alpha}}\boldsymbol{\theta} + \left(1 + \frac{1}{\omega_n}\sqrt{\frac{F_\alpha}{2\|\boldsymbol{\theta}\|_\alpha}}\right)\boldsymbol{\omega}\right] - \boldsymbol{\alpha}_{\mathbf{D}} \tag{70}$$

for the angular deceleration region, and

$$\boldsymbol{\alpha}_{\mathbf{C}} = -\omega_n\left[\frac{F_\omega}{\|\boldsymbol{\theta}\|_\omega}\boldsymbol{\theta} + \boldsymbol{\omega}\right] - \boldsymbol{\alpha}_{\mathbf{D}} \tag{71}$$

for the angular rate limit region.

Note that, with $\boldsymbol{\theta}$ approaching zero, both controls are not applicable, since their gains reach infinity. An additional equation for the small values of $\boldsymbol{\theta}$ must therefore be developed. When $\|\boldsymbol{\theta}\|$ approaches zero, the kinematics are reduced to $\dot{\boldsymbol{\theta}} = \boldsymbol{\omega}$. This is the region where the bandwidth constraint is dominant. According to [4,15], the following linear second-order controller is used when $\|\boldsymbol{\theta}\|$ becomes smaller than some threshold.

Linear zone:

$$\boldsymbol{\alpha}_{\mathbf{C}} = -\omega_n[\omega_n\boldsymbol{\theta} + 2\zeta\boldsymbol{\omega}] - \boldsymbol{\alpha}_{\mathbf{D}} \tag{72}$$

The threshold as well as the damping coefficient ζ are discussed in the next subsection.

F. Switching Conditions Between Different Controls

To keep the controller cascaded structure, the switching criteria should be a function of $\boldsymbol{\theta}$, just like the braking curve $\mathbf{f}(\boldsymbol{\theta})$. Three borders have to be established: 1) angular rate limit zone to angular deceleration limit zone, 2) angular deceleration limit zone to linear zone, and 3) angular rate limit zone to linear zone.

1. Border Between Angular Rate Limit Zone and Angular Acceleration Limit Zone

It is evident from Eq. (11) that maneuvering with constant (maximum) angular rate requires a control acceleration that is equal to $-\boldsymbol{\alpha}_{\mathbf{D}}$. For smooth switching, the border is thus set where both control equations (70) and (71) would provide $-\boldsymbol{\alpha}_{\mathbf{D}}$. Therefore, $\boldsymbol{\theta}$ in Eq. (70) is replaced with $-(\|\boldsymbol{\theta}\|_\omega/F_\omega)\boldsymbol{\omega}$, which is attained from Eq. (71) after replacing $\boldsymbol{\alpha}_C$ with $-\boldsymbol{\alpha}_{\mathbf{D}}$. This requires

$$0 = -\omega_n\left[-\sqrt{\frac{2F_\alpha}{\|\boldsymbol{\theta}\|_\alpha}}\frac{\|\boldsymbol{\theta}\|_\omega}{F_\omega} + \left(1 + \frac{1}{\omega_n}\sqrt{\frac{F_\alpha}{2\|\boldsymbol{\theta}\|_\alpha}}\right)\right]\boldsymbol{\omega}$$

Using the knowledge that, during the angular deceleration phase, the right-hand term of the preceding equation (which is the net acceleration) should be opposite to $\boldsymbol{\omega}$, we conclude that when the multiplier

$$-\sqrt{\frac{2F_\alpha}{\|\boldsymbol{\theta}\|_\alpha}}\frac{\|\boldsymbol{\theta}\|_\omega}{F_\omega} + \left(1 + \frac{1}{\omega_n}\sqrt{\frac{F_\alpha}{2\|\boldsymbol{\theta}\|_\alpha}}\right)$$

is positive (i.e., the deceleration limit region), we should use the control according to Eq. (70), whereas when it is negative (i.e., the angular rate limit region), we should use the control of Eq. (71). This yields the following inequality defining the condition for controlling according to Eq. (71) rather than Eq. (70):

$$\|\boldsymbol{\theta}\|_\omega/F_\omega > \sqrt{\|\boldsymbol{\theta}\|_\alpha/(2F_\alpha)} + 1/(2\omega_n) \tag{73}$$

Table 2 Control law summary

Control equation	Gain values	Conditions (inequalities number)	Motion type
Equation (70)	$\omega_n = \omega_{n_{\text{Basic}}}$	Equation (74) and not Eq. (73)	Angular deceleration limited
Equation (71)	$\omega_n = \omega_{n_{\text{Basic}}} \times 3/2$	Equations (73) and (77)	Angular rate limited
Equation (72)	$\omega_n = \omega_{n_{\text{Basic}}}, \zeta = 3/4$	{Eq. (73) and not Eq. (77)} or {not Eq. (73) and not Eq. (74)}	Target tracking

2. Border Between Linear Zone to Angular Deceleration Limit Zone

Comparing the angular gains between Eqs. (70) and (72), and choosing the minimum gain from the two, results in the following inequality that defines the condition for controlling according to Eq. (70) rather than Eq. (72):

$$\|\boldsymbol{\theta}\|_\alpha > 2F_\alpha/\omega_n^2 \tag{74}$$

Now, equating the angular rate gains of Eqs. (70) and (72) at the border point gives

$$2\zeta\omega_n = \omega_n\left(1 + \frac{1}{\omega_n}\sqrt{\frac{F_\alpha}{2\|\boldsymbol{\theta}_{\mathbf{Border_2}}\|_\alpha}}\right) \tag{75}$$

where $\|\boldsymbol{\theta}_{\mathbf{Border_2}}\|_\alpha$ is replaced with $2F_\alpha/\omega_n^2$ according to Eq. (74) to provide the coefficient ζ:

$$\zeta = \tfrac{3}{4} \tag{76}$$

3. Border Between Linear Zone and Angular Rate Limit Zone

As mentioned, maneuvering with constant (maximum) angular rate requires a control acceleration that is equal to $-\boldsymbol{\alpha}_\mathbf{D}$. The border is thus set where both control equations (71) and (72) would provide $-\boldsymbol{\alpha}_\mathbf{D}$. Replacing $\boldsymbol{\theta} = -(\|\boldsymbol{\theta}\|_\omega/F_\omega)\boldsymbol{\omega}$, attained from Eq. (71), in Eq. (72) and replacing ζ from Eq. (76) gives $0 = -\omega_n(-\omega_n\|\boldsymbol{\theta}\|_\omega/F_\omega + 3/2)\boldsymbol{\omega}$. As in the case of the first border, the multiplier $(-\omega_n\|\boldsymbol{\theta}\|_\omega/F_\omega + 3/2)$ must be positive when switching to linear control. This yields the third inequality defining the condition for controlling according to Eq. (71) rather than Eq. (72):

$$\|\boldsymbol{\theta}\|_\omega > 3F_\omega/(2\omega_n) \tag{77}$$

Comparison between the angular rate gains of Eqs. (71) and (72) shows that if the gain of Eq. (71) is multiplied by the term 2ζ, then gain continuity can be guaranteed. The gain ω_n is thus not common to all three Eqs. (70–72). The common ω_n for both Eqs. (70) and (72) will thus be denoted as $\omega_{n_{\text{Basic}}}$. A different ω_n is applied in Eq. (71). At this point, the control law may be summarized by Table 2.

G. Control Saturation Management

In general, the initial system state is far from the braking curve, such that the control equation (43) usually results in an excessive acceleration demand. The maneuver thus generally starts with saturated control (see Fig. 5) that lasts until the state becomes close enough to the braking curve. The state then exponentially approaches and tracks the braking curve according to Eq. (46) until $\boldsymbol{\theta}$ is small enough to apply the linear control. During the saturated control stage, it is important to maintain the validity of Eq. (47), which is the analytical basis of our control equations, while limiting the control to the available envelope. Analysis of Eqs. (70–72) shows that the only variable that may not stay in the plane $\boldsymbol{\theta} - \boldsymbol{\omega}$ is $\boldsymbol{\alpha}_\mathbf{D}$. Consequently, it is proposed to divide all the other elements by the appropriate factor, while the disturbance compensation element $\boldsymbol{\alpha}_\mathbf{D}$ remains unchanged, allowing Eq. (47) to remain valid. This method of control saturation is called basic saturation management (BSM). This approach can be taken further, such that the sum $\boldsymbol{\alpha}_\mathbf{FF} - \boldsymbol{\alpha}_\mathbf{D}$ is kept unchanged and only the scalar gain ω_n would be reduced according to the saturation level at any given time. This modified saturation method is referred to as

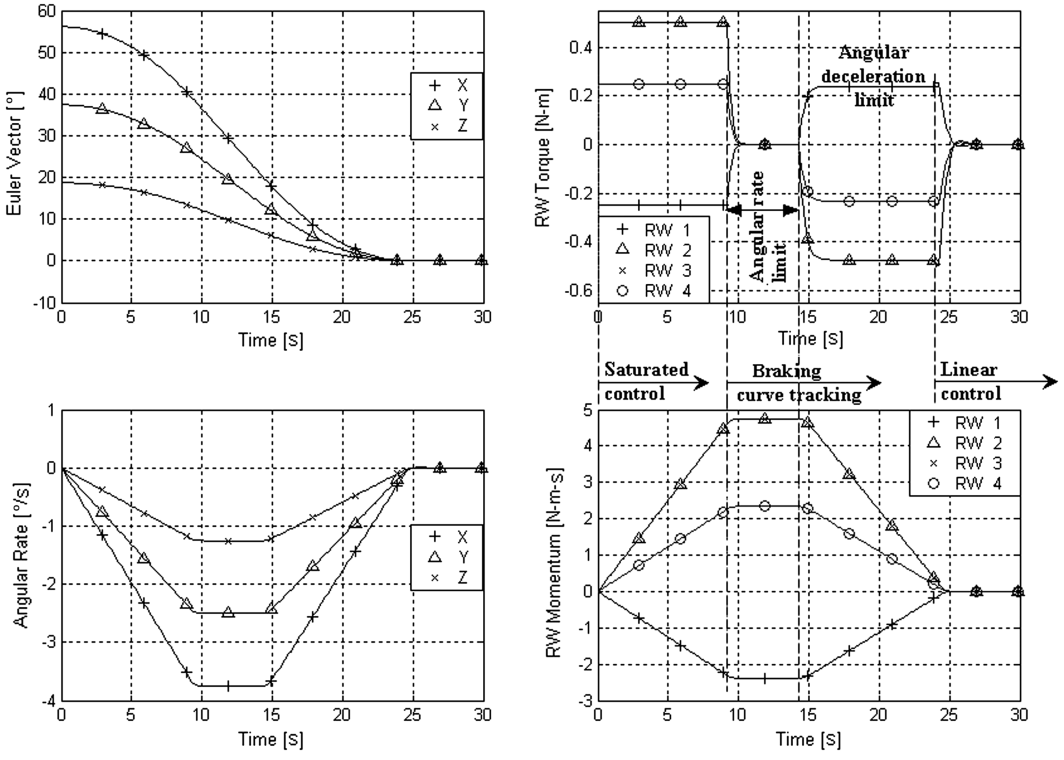

Fig. 5 Typical rest-to-rest maneuver with angular rate limit encountered (same results for BSM and ASM).

Table 3 Simulation parameters

Parameter name	Parameter meaning	Parameter value
h_{Limit_i}	Limit angular momentum of each RW	5 N · m · s
T_S	Sampling time of control loop	0.1 s
$\omega_{n_{\text{Basic}}}$	Control gain	2.5 rad/s
F_α	Ratio between safe and maximum decelerations	0.85–0.95 (default is 0.95)
F_ω	Ratio between safe and maximum angular rates	0.95

the advanced saturation management (ASM). Both BSM and ASM are tested by simulation and compared in the next section.

To sum up this subsection, the saturation management equations are summarized next. Based on the general control equation (43), the saturation case can be defined as follows:

$$\boldsymbol{\alpha}_{\mathbf{Saturated}} = \omega_n[\mathbf{f}(\boldsymbol{\theta}) - \boldsymbol{\omega}] + \boldsymbol{\alpha}_{\mathbf{FF}} - \boldsymbol{\alpha}_{\mathbf{D}}, \quad \text{where } \|\boldsymbol{\alpha}_{\mathbf{Saturated}}\|_\alpha > 1 \tag{78}$$

The BSM saturation management method gives

$$\boldsymbol{\alpha}_{\mathbf{C}} = \frac{\omega_n(\mathbf{f}(\boldsymbol{\theta}) - \boldsymbol{\omega}) + \boldsymbol{\alpha}_{\mathbf{FF}}}{\lceil \omega_n(\mathbf{f}(\boldsymbol{\theta}) - \boldsymbol{\omega}) + \boldsymbol{\alpha}_{\mathbf{FF}}, -\boldsymbol{\alpha}_{\mathbf{D}} \rceil_\alpha} - \boldsymbol{\alpha}_{\mathbf{D}}, \quad \text{where} \lceil \ldots \rceil_\alpha \text{ is calculated with } F_\alpha = 1 \tag{79}$$

The ASM saturation management method gives

$$\boldsymbol{\alpha}_{\mathbf{C}} = \frac{\mathbf{f}(\boldsymbol{\theta}) - \boldsymbol{\omega}}{\lceil \mathbf{f}(\boldsymbol{\theta}) - \boldsymbol{\omega}, \boldsymbol{\alpha}_{\mathbf{FF}} - \boldsymbol{\alpha}_{\mathbf{D}} \rceil_\alpha} + \boldsymbol{\alpha}_{\mathbf{FF}} - \boldsymbol{\alpha}_{\mathbf{D}}, \quad \text{where } \lceil \ldots \rceil_\alpha \text{ is calculated with } F_\alpha = 1 \tag{80}$$

V. Simulation Results

The main purpose of this section is to demonstrate the efficiency of the newly developed control logic that has been presented in the previous sections by using a practical numerical example. Simulated closed-loop angular maneuvers are presented and analyzed with various realistic initial conditions and target angular rates. The simulations follow from the numerical example of Sec. III.B. Only the $L\infty$ method for control allocation is applied in the presented simulations due to its significant advantage (see Sec. III.B). Results for both saturation management methods (BSM and ASM) are presented.

A. Simulations

The simulations used realize finite time steps with the following three coupled elements: 1) satellite dynamics and kinematics, which are realized using the equations of motion of rigid satellite with RWs, as presented in Sec. II; 2) the control law as presented in Sec. IV; and 3) the torque command allocation of the $L\infty$ method as defined in Secs. III.A and III.B.

B. System Parameters

The parameters have been presented in the numerical example of Sec. III.B. Additional parameters are listed in Table 3.

C. Performance Criteria

Following Sec. I, the criteria used to assess the performance of the newly developed control logic in the simulated maneuvers are based on the following:

1) The controller should abide by the RW torque and angular momentum limits.

2) For time efficiency, the maneuver time for the rest-to-rest and zero momentum bias case should be as close to the time-optimal Euler-axis rotation as the system bandwidth and the disturbance allocation (i.e., safety factors) allow.

3) The last deceleration phase of the maneuver (where the sliding curve is tracked) should be free of control saturation and free of chattering.

4) Any initial angular rate within the limit envelope is allowed.

5) The final angular rate within the limit envelope is allowed, as long as the resulting cross disturbance [Eq. (10)] does not exceed the control limit.

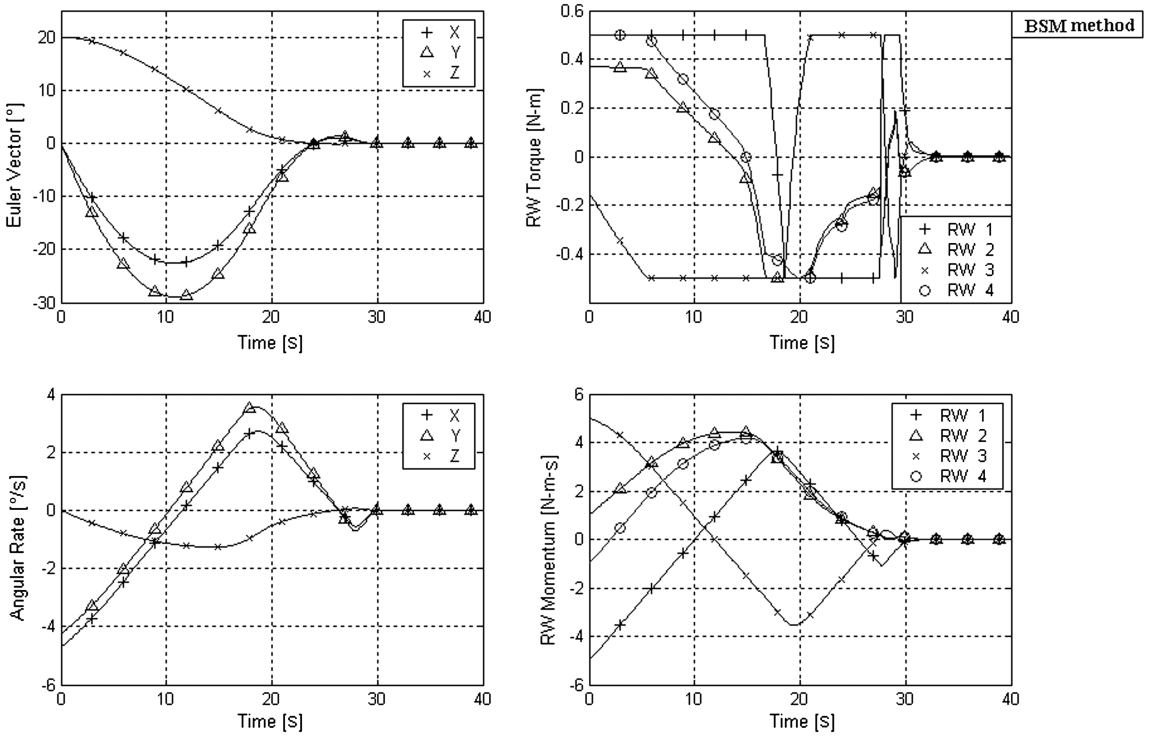

Fig. 6 Maneuver with initial cross-angular rate: BSM method saturation.

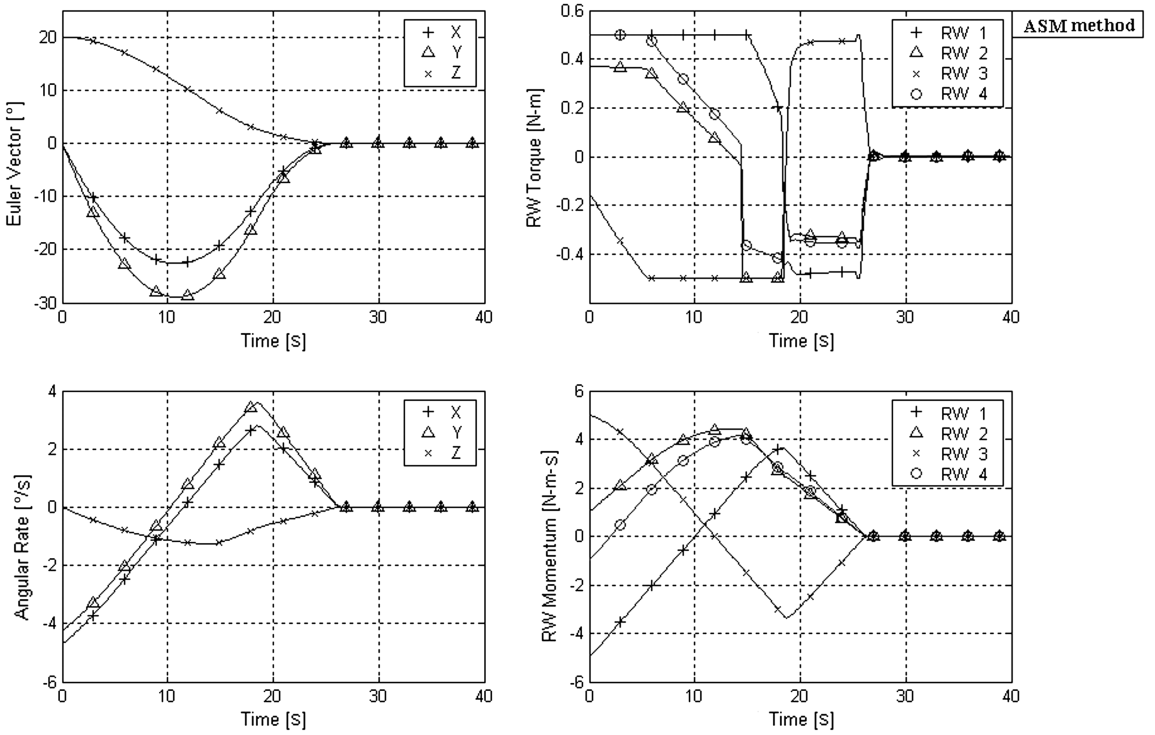

Fig. 7 Maneuver with initial cross-angular rate: ASM method saturation.

D. Summary

All plots describe one attitude maneuver. The following data are plotted as functions of time: 1) satellite BF Euler vector relative to TF, 2) satellite BF angular rate vector relative to TF, 3) torque command of each of the four RWs to ensure/validate the full exploitation of torque capability (when maximum torque is required, at least two RWs will simultaneously be close to the torque limit), and 4) angular momentum of each of the four RWs to validate the full exploitation of the angular rate capability. Similarly, when maximum angular rate is required, at least two RWs will simultaneously be close to the angular momentum limit. The scenarios simulated are presented in Table 4 together with the maneuver time.

E. Typical Rest-to-Rest Maneuver that Reaches the Angular Rate Limit

Figure 5 presents a rest-to-rest maneuver that involves the X, Y, and Z axes together. The results of both BSM and ASM methods are identical in the rest-to-rest case. Referring to the performance criteria of Sec. V.C, the first three criteria are obviously met, and the other two are irrelevant to the scenario tested. This maneuver, as well as all the other maneuvers simulated using this controller, consists of three stages:

1) In the stage of the convergence to the braking curve, the control torque is in saturation, which means that at least two RWs (typical to $L\infty$ control allocation) are on the limit torque.

2) In the braking-curve tracking stage, the braking curve dictates an Euler-axis time-optimal rotation with safe angular rate and deceleration, which is tracked. The control torque during this stage is normally not saturated, since the design is for safe angular deceleration.

3) In the linear control stage, after convergence of the system state to the near origin, the bandwidth limit becomes the major constraint, and the system is linearly controlled with constant gains. The trapezoid or triangular shape (the triangle is produced when the angular rate limit is not reached) of the angular rate profiles, as well as the control torque saturation of the first stage and the near saturation of the second stage, are evidence of an eigenaxis time-optimal maneuver taking place. The round corners of the angular rate profiles are due to the system bandwidth limit.

Table 4 Simulation cases

Figure/section	Simulation scenarios		Performance, s
Fig. 5/Sec. V.E	Typical rest-to-rest maneuver with angular rate limit encountered		24.7
Figs 6 and 7/Sec. V.F	Maneuver with initial cross-angular rate: comparison between BSM to ASM	BSM method	29.6
		ASM method	26.1
Figs 8–10/Sec. V.G	Maneuver with initial cross-bias angular momentum: ASM method.	$F_\alpha = 0.95$	17.3
		$F_\alpha = 0.85$	13.9
		$F_\alpha = 0.85$ Only 80% of $\boldsymbol{\alpha}_D$ is accounted for	14.1
Figs 11 and 12/Sec. V.H	Maneuver with nonzero end angular rate: ASM method.	$F_\alpha = 0.95$	12.8
		$F_\alpha = 0.85$	10.8
Fig. 13/Sec. V.I	Maneuver with parameters mismatch between control system and reality: ASM method.	$F_\alpha = 0.95$	24.3
[a]/Sec. V.J	Maneuver with too conservative safety factor	$F_\alpha = 0.85$	25.3

[a]Plots are visually very similar to Fig. 5 and, consequently, are not presented

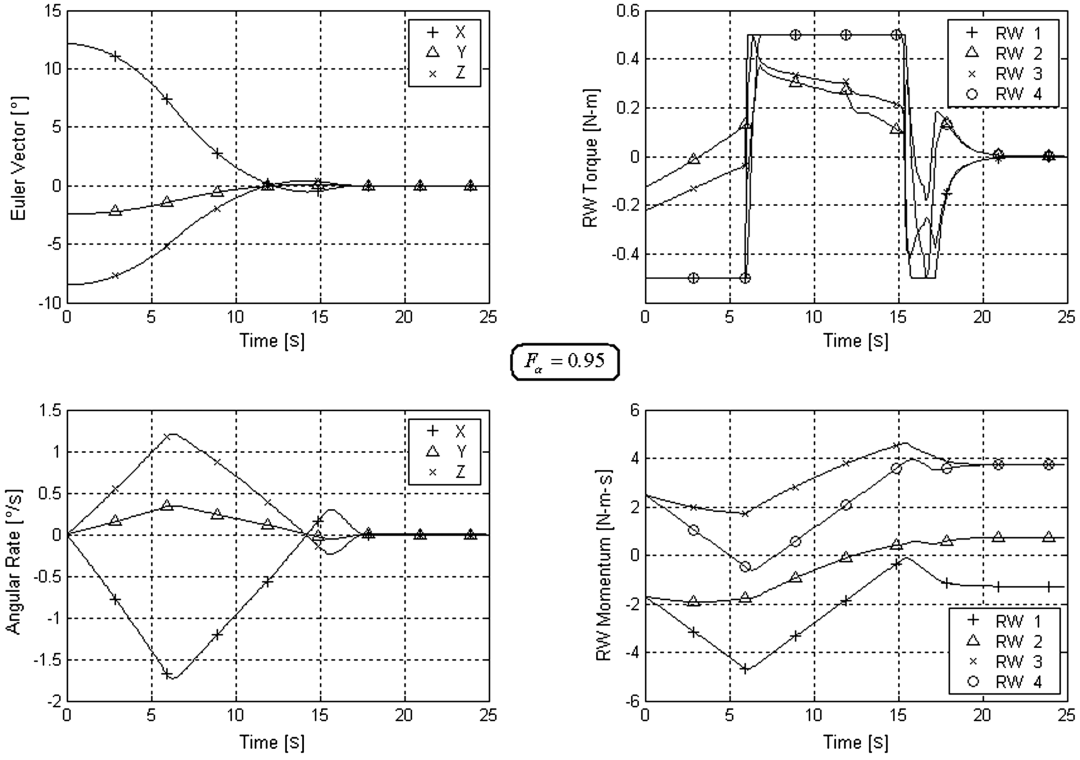

Fig. 8 Maneuver with initial cross-angular momentum bias, $F_\alpha = 0.95$.

F. Maneuver with Initial Cross-Angular Rate

Figures 6 and 7 depict a maneuver that begins with an angular rate that is perpendicular to the initial Euler axis but with zero total angular momentum. Figure 6 presents the results with the BSM case, whereas Fig. 7 presents the results for the ASM case. It can be observed that the ASM has a 13% advantage in the maneuvering time in this case (see Table 4). This is because the BSM misses the braking curve on the first trial, resulting in an overshoot. As for the performance criteria of Sec. V.C, the first, third, and fourth criteria are satisfied with both the BSM and ASM versions. The second and fifth criteria are irrelevant to this tested scenario.

G. Maneuver with Cross-Angular Momentum Bias

As shown in Eq. (10), the existence of angular momentum bias in the system creates a disturbance angular acceleration when coupled

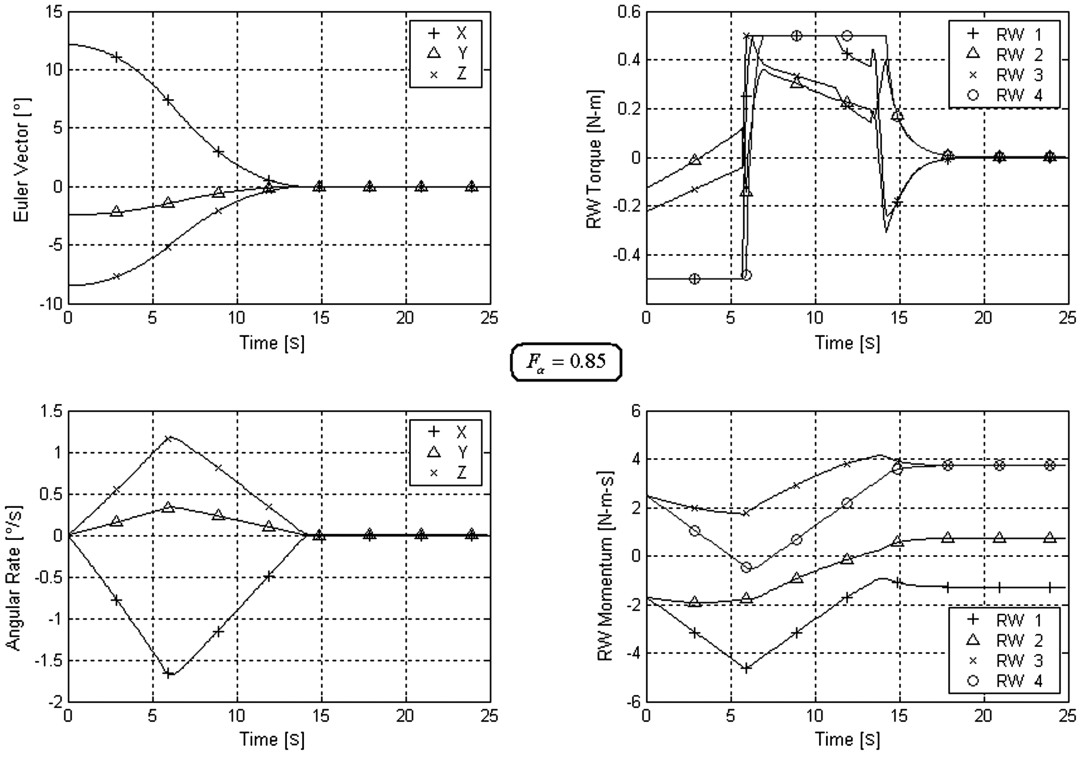

Fig. 9 Maneuver with initial cross-angular momentum bias, $F_\alpha = 0.85$.

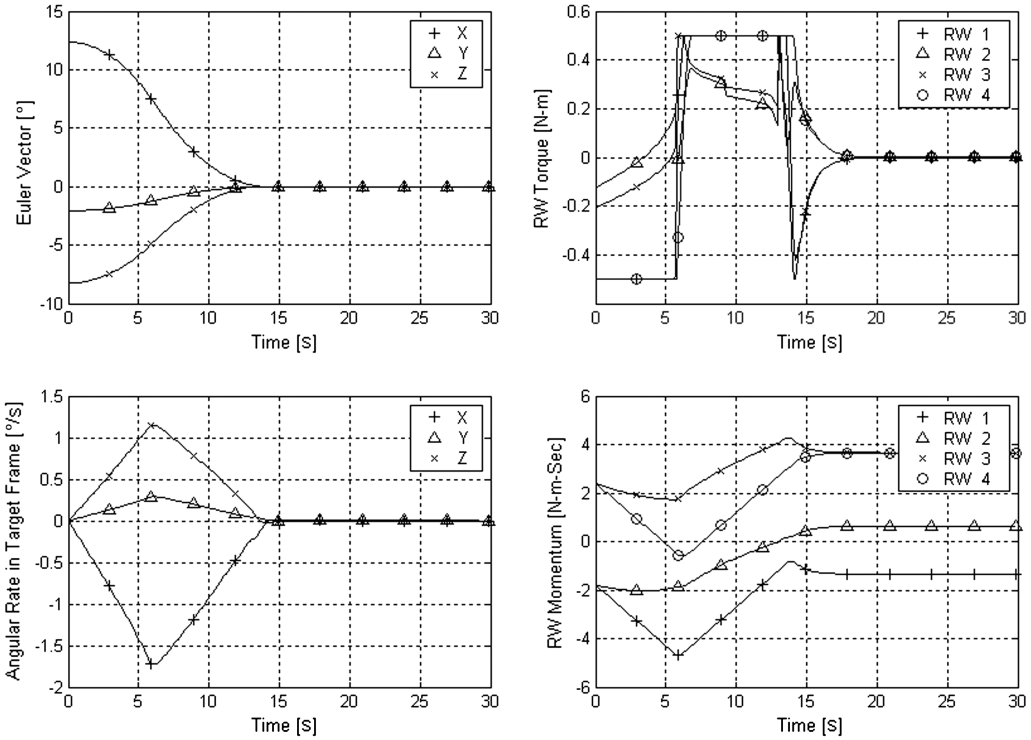

Fig. 10 Maneuver with the same conditions as Fig. 9, including 20% disturbance compensation error.

with satellite angular rates. This can disable the braking-curve tracking capability if an appropriate safety factor F_α is not taken, as explained in Sec. III.A.3.

Figures 8 and 9 show the results with the ASM method: first with a value of $\boldsymbol{F_\alpha} = 0.95$ and then with a modified value that allows safe braking-curve tracking. It can be observed that the case with the modified $\boldsymbol{F_\alpha}$ has a 20% advantage in maneuver time (see Table 4). However, it must be stressed that using a decreased safety factor does provide a benefit only when a disturbance actually occurs. Choosing the same safety factor in a low disturbance torque case would degrade the performance attained due to the reduction of the braking-curve deceleration (see Sec. V.J). Therefore, this safety factor needs to be adjusted according to the actual disturbance level range.

An additional scenario is presented with the same conditions as in Fig. 9 to test the robustness against inaccuracy in the disturbance compensation $\boldsymbol{\alpha}_D$. In this additional scenario, only 80% of the actual disturbance $\boldsymbol{\alpha}_D$ was accounted for by the control law. As seen in Fig. 10, this inaccuracy did not significantly affect the time response, and the maneuver time is increased by only 1.4% (see Table 4).

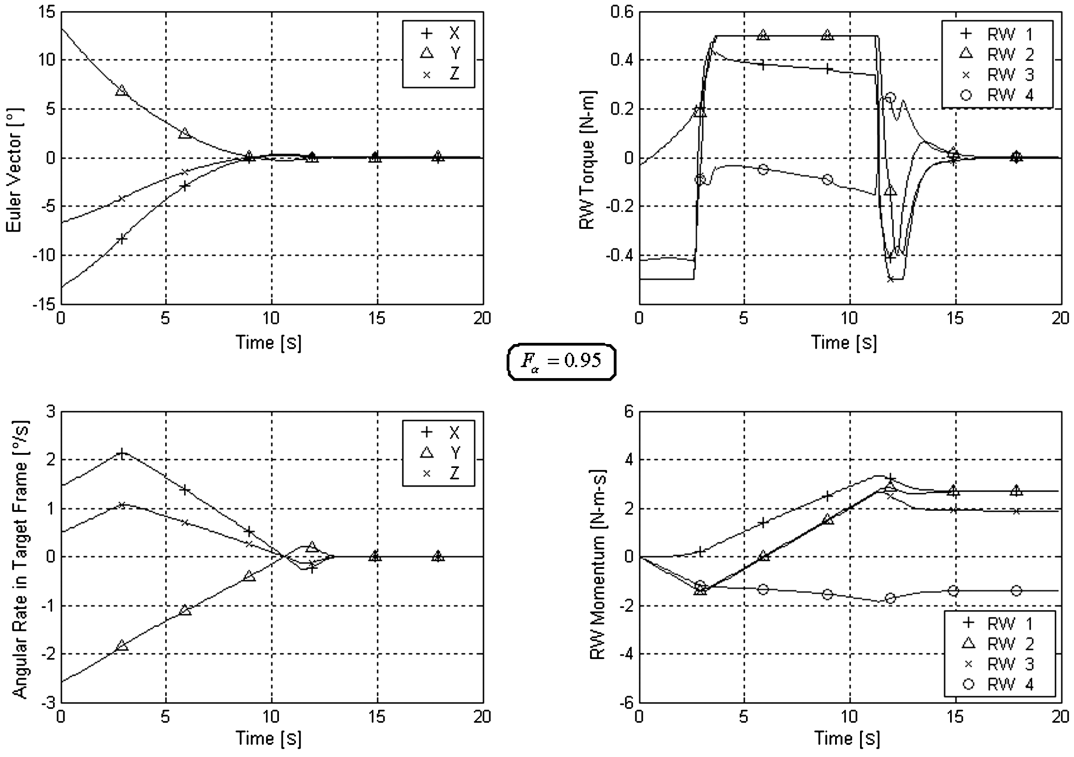

Fig. 11 Maneuver with nonzero end angular rate, $F_\alpha = 0.95$.

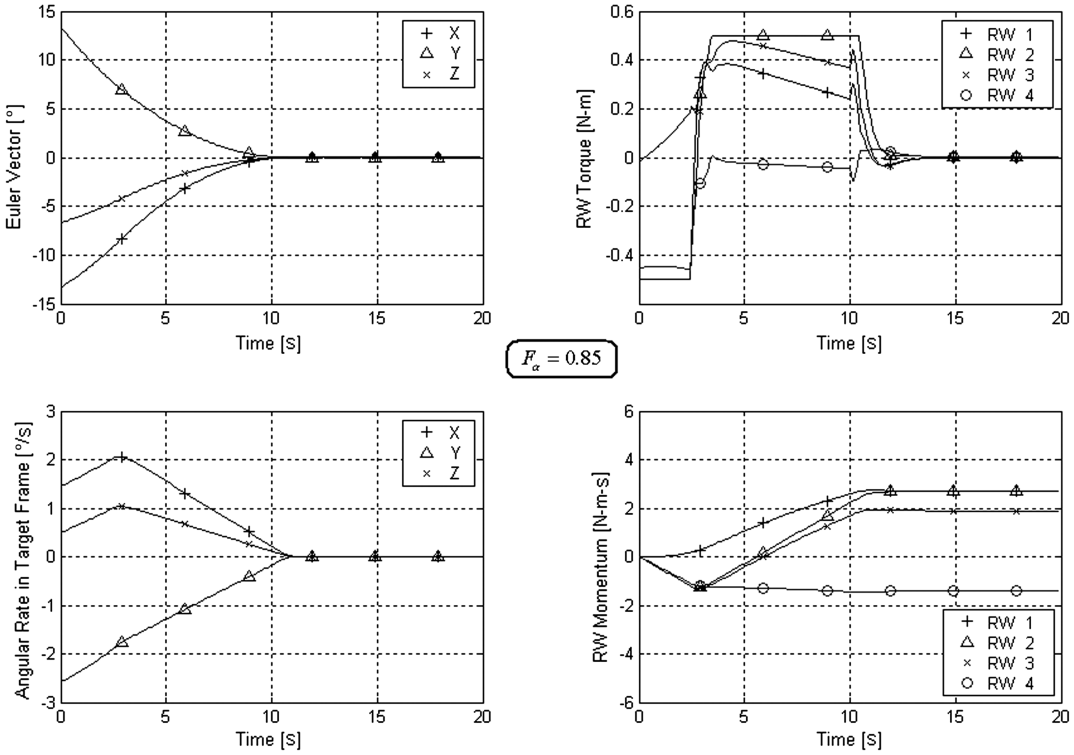

Fig. 12 Maneuver with nonzero end angular rate, $F_\alpha = 0.85$.

H. Maneuver with Nonzero End Angular Rate

The existence of final angular rate (which is the target angular rate) creates a disturbance in angular acceleration when coupled with the satellite's angular rate [Eq. (10)]. This can disable the braking-curve tracking capability if an appropriate safety factor F_α is not considered, as explained in Sec. III.A.3. Figures 11 and 12 show the results of the ASM method: first by using a default value of $F_\alpha = 0.95$ and then by using a modified value that allows safe braking and curve tracking. It can be observed that the case with a modified F_α has a 16% advantage in the maneuvering time (see Table 4). Similar to the previous scenario, the safety factor has to be carefully adjusted according to the actual disturbance level range. In the case of low disturbances, the small safety factor provides inferior time performance, because smaller braking deceleration is generated (see Sec. V.J).

I. Maneuver with Parameter Mismatch

The following scenario demonstrates the system reaction when a mismatch exists between the moments of inertia used in the control law compared with the actual values. This is done to simulate

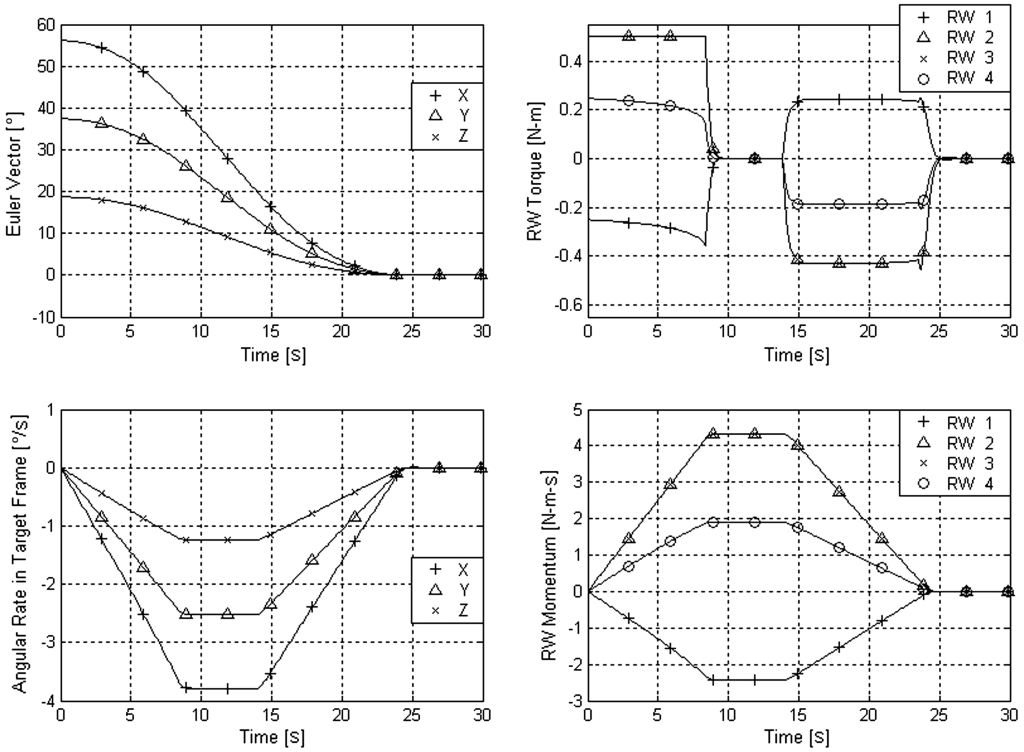

Fig. 13 Maneuver with moment of inertia mismatch between controller to reality.

potential parameter uncertainties. The typical rest-to-rest scenario of Fig. 5 was repeated with the actual moments of inertia decreased 5% in the X axes, 10% in the Y axes, and 15% in the Z axes. Note that increasing the moments of inertia would require a smaller safety factor, but decreasing them increases the available angular acceleration, and thus does not require the safety factor to be changed. The results are presented in Fig. 13, which shows that, despite the nonuniform inertia change, the maneuver is very similar to the original in Fig. 5. As expected, the control effort (RW torques and angular momentum) in the braking-curve tracking stage 2 (see Sec. V.E) is smaller than in Fig. 5 because of the smaller inertias.

J. Maneuver with Too Conservative Safety Factor

This scenario demonstrates the system reaction with a too conservative safety factor F_α. The typical rest-to-rest scenario of Sec. V.E was repeated with $F_\alpha = 0.85$ rather than 0.95. The result is presented in Table 4, which shows a relatively small penalty of 2.4% in the maneuvering time. As mentioned in Secs. V.G and V.H, the safety factors should be adjusted according to the actual disturbance level range proposed in Sec. III.A.3, Eqs. (28) and (29). However, the performance penalty for a too conservative factor is usually smaller than the penalty resulting from a factor that is too close to unity (as demonstrated by this example versus Secs. V.G and V.H).

VI. Conclusions

The aim of this paper is to present an enhanced RW controller that bridges the gaps that have been identified in the literature. The main novelty of the proposed controller is the use of a generalized and integrative approach, where most common system limits and possible conditions are referred, while also placing an emphasis on time efficiency. The presented technique accommodates for the RW torque and angular rate limits and their 3-D geometrical alignment, which are all formulated in two compact control norm expressions for the satellite angular acceleration and angular rate. The system bandwidth limit is accommodated by choosing an appropriate control gain, thus avoiding the need of using any switching between maximum and minimum controls, as is commonly done in minimum time solutions, which may lead to undesirable control chattering in practical applications. The applicability of the solution for cases of nonzero initial angular rate and nonzero end angular rate, as well as nonzero angular momentum bias, has been demonstrated in realistic simulations, showing the flexibility and the efficiency of the new integrated control logic. The importance of tuning the safety factor related to the actual disturbance level has been demonstrated. The selected tuning factor should be sufficiently small to accommodate for possible disturbances but not too small in order to avoid any sacrifice in performance.

References

[1] Wie, B., and Lu, J., "Feedback Control Logic for Spacecraft Eigenaxis Rotations Under Slew Rate and Control Constraints," *Journal of Guidance, Control, and Dynamics*, Vol. 18, No. 6, Nov–Dec 1995, pp. 1372–1379. doi:10.2514/3.21555

[2] Bilimoria, K. D., and Wie, B., "Time-Optimal Three-Axis Reorientation of a Rigid Spacecraft," *Journal of Guidance, Control, and Dynamics*, Vol. 16, No. 3, May–June 1993, pp. 446–452. doi:10.2514/3.21030

[3] Fleming, A., Sekhavat, P., and Ross, M., "Minimum-Time Reorientation of a Rigid Body," *Journal of Guidance, Control, and Dynamics*, Vol. 33, No. 1, Jan.–Feb. 2010, pp. 160–170. doi:10.2514/1.43549

[4] Wie, B., Weiss, H., and Arapostathis, A., "Quaternion Feedback Regulator for Spacecraft Eigenaxis Rotations," *Journal of Guidance, Control, and Dynamics*, Vol. 12, No. 3, 1989, pp. 375–380. doi:10.2514/3.20418

[5] Byers, R. M., and Vadali, S. R., "Quasi-Closed-Form Solution to the Time-Optimal Rigid Spacecraft Reorientation Problem," *Journal of Guidance, Control, and Dynamics*, Vol. 16, No. 3, May–June 1993, pp. 453–461. doi:10.2514/3.21031

[6] Steyn, W. H., "Near-Minimum-Time Eigenaxis Rotation Maneuvers Using Reaction Wheels," *Journal of Guidance, Control, and Dynamics*, Vol. 18, No. 5, 1995, pp. 1184–1189. doi:10.2514/3.21523

[7] Etter, J. R., "A Solution of the Time Optimal Euler Rotation Problem," AIAA Paper 1989-3601, Aug. 1989.

[8] Xiaojiang, C., and Steyn, W. H., "Robust combined eigenaxis slew maneuvers," AIAA Guidance Navigation and Control Conference, AIAA Paper 1999-4048, Aug. 1999.

[9] Newman, W. S., "Robust Near Time-Optimal Control (of double integrator plant)," *IEEE Transactions on Automatic Control*, Vol. 35, No. 7, July 1990, pp. 841–844. doi:10.1109/9.57026

[10] Dodds, S. J., and Vittek, J., "Spacecraft Attitude Control Using an Induction Motor Actuated Reaction Wheel with Sensorless Forced Dynamic Drive," *IEE Colloquium on All Electric Aircraft*, Vol. 1998/26017 June 1998, pp. 9/1–9/7.

[11] Zwartbol, T., van den Dam, R. F., Terpstra, A. P., and van Woerkom, P. T. L. M., "Attitude Estimation and Control of Maneuvering Spacecraft," *Automatica*, Vol. 21, No 5, 1985, pp. 513–526. doi:10.1016/0005-1098(85)90001-9

[12] Crassidis, J. L., Vadali, S. R., and Markley, F. L., "Optimal Variable Structure Control Tracking of Spacecraft Maneuvers," *Journal of Guidance, Control, and Dynamics*, Vol. 23, No. 3, 2000, pp. 564–566. doi:10.2514/2.4568

[13] Kim, J., and Crassidis, J. L., "A Comparative Study of Sliding Mode Control and Time-Optimal Control," AIAA/AAS Astrodynamics Specialist Conference, Boston, AIAA Paper 1998-4473, Aug. 1998.

[14] Lawton, J., and Beard, R. W., "Attitude Regulation About a Fixed Rotation Axis," *Journal of Guidance, Control, and Dynamics*, Vol. 26, No. 2, 2003, pp. 253–258. doi:10.2514/2.5066

[15] Wie, B., Bailey, D., and Heiberg, C., "Rapid Multitarget Acquisition and Pointing Control of Agile Spacecraft," *Journal of Guidance, Control, and Dynamics*, Vol. 25, No. 1, Jan.–Feb. 2002, pp. 96–104. doi:10.2514/2.4854

[16] Kane, T. R., Levinson, D. A., and Likins, P. W., "Simple Spacecraft," *Spacecraft Dynamics*, McGraw–Hill, New York, 1983, pp. 159–246.

[17] Verbin, D., and Ben-Asher, J. Z., "Time Efficient Closed Loop Steering Laws for Rigid Satellite Large Rotational Maneuver," AIAA Guidance, Navigation, and Control Conference, Keystone CO, AIAA Paper 2006-6042, 2006.

[18] Sidi, M. J., "Attitude Maneuvers in Space," *Spacecraft Dynamics and Control: A Practical Engineering Approach*, 1st ed., Cambridge Univ. Press, New York, 1997, pp. 173, 195–209.